Resource Allocation for Multi-IoT-Node Mutualistic Symbiotic Radio with Hybrid Long and Short Packets

Liqin Shi, Yinghui Ye, *Member, IEEE*, Xiaoli Chu, *Senior Member, IEEE*, Guangyue Lu, and Sumei Sun, *Fellow, IEEE*

***Abstract*—Mutualistic symbiotic radio (MSR) that allows a primary link and a backscatter link to share resources and benefit each other has been investigated mainly for long-packet communications. In the Internet of Things (IoT), where short packets are often transmitted, the design of MSR needs to consider the distinct features of short packet transmissions. In this work, we study a multi-IoT-node MSR network supporting both long and short packet transmissions, where a primary transmitter sends long packets to a cooperative receiver (CR), while multiple IoT nodes sequentially backscatter their short packets to the CR. We first derive the lower bound expression for the primary transmission rate by considering the error probabilities (EPs) of the IoT nodes' short-packet communications. On this basis, we propose a resource allocation scheme to maximize the weighted sum throughput of all IoT nodes, subject to the constraints on the quality-of-service requirement and energy causality for each IoT node, as well as the throughput gain for the primary transmission. Specifically, the weighted sum throughput maximization problem is formulated by jointly optimizing the short-packet blocklength, power reflection coefficient and EP of each IoT node, and is solved by proposing an iterative algorithm based on the block coordinate decent method. Simulation results confirm the quick convergence of the proposed iterative algorithm and show that our proposed scheme outperforms the existing scheme in terms of the weighted sum throughput of all IoT nodes.**

***Index Terms*—Mutualistic symbiotic radio, short-packet communications, resource allocation.**

I. INTRODUCTION

WITH the rapid evolution of services and applications in the era of the Internet of Things (IoT), it is anticipated that over 80 billion low-power devices will be deployed globally by 2030 [1]. This unprecedented growth in IoT calls for spectrum- and energy-efficient communication technologies. A promising technology is the backscatter communications (BackCom)-enabled symbiotic radio (SR), in which a low-power IoT device injects its information into an incident radio frequency (RF) signal broadcast by a primary transmitter (PT) and then reflects the modulated signal to its receiver while simultaneously harvesting energy from the incident signal by adjusting its power reflection coefficient (PRC) [2], [3]. SR brings two advantages. One is the spectrum sharing between the primary and backscatter links, improving spectrum efficiency. The other is the near-zero power consumption of IoT nodes due to the passive BackCom that does not require any high-power components for carrier generation.

There have been two setups for SR, namely parasitic SR (PSR) and mutualistic SR (MSR). Specifically, in PSR, the symbol duration of the primary signal is the same as or comparable to that of the backscattered signal. In this case, the cooperative receiver (CR) first decodes the PT's information by treating the IoT node's BackCom signal as interference and then decodes the IoT node's information after subtracting the PT's signal from the received signal. In MSR, the symbol duration of the primary signal is much shorter than that of the backscattered signal. Due to the backscatter process, the backscattered signal carries information from both the PT and the IoT node. Thus, the backscatter link can be regarded as an additional multipath for the primary information with a slow channel variation introduced by the adjustment of the PRC at the IoT node. In this case, the IoT node can obtain the transmission opportunity without requiring additional spectrum or energy resources. In return, the IoT node's BackCom provides a multipath gain rather than interference to the primary transmission, thereby enhancing the performance of the primary transmission. As a result, mutual benefits arise between the primary and backscatter links, forming a mutualistic relationship between them [4]–[6].

Both PSR and MSR have garnered considerable interest. The authors in [5] maximized the weighted sum rate of the primary and backscatter transmissions and minimized the PT's transmit power for both PSR and MSR networks. Different from [5] that considered a single IoT node, the authors in [7] maximized the energy efficiency (EE) of PSR and MSR for multiple IoT nodes, respectively. The authors in [4] revealed that the symbol period ratio enabling mutualistic symbiosis in MSR is not related to specific channel realizations but is instead determined by the average strengths of the primary and backscatter links when the number of receiving antennas is large. Considering hardware impairments (HIs) at all the active

The work of Liqin Shi was supported in part by the National Natural Science Foundation of China under Grant 62301421 and in part by the Young Talent Fund of University Association for Science and Technology in Shaanxi under Grant 20250114. The work of Yinghui Ye was supported in part by the National Natural Science Foundation of China under Grant 62201451 and in part by the Innovation Capability Support Program of Shaanxi under Grant 2024ZC-KJXX-016. (*Corresponding author: Yinghui Ye.*)

Liqin Shi, Yinghui Ye and Guangyue Lu are with the Shaanxi Key Laboratory of Information Communication Network and Security, Xi'an University of Posts & Telecommunications, China. (email: liqinshi@hotmail.com; connectyyh@126.com; tonylugy@163.com)

Xiaoli Chu is with the Department of Electronic and Electrical Engineering, The University of Sheffield, U.K. (e-mail: x.chu@sheffield.ac.uk)

Sumei Sun is with the Institute of Infocomm Research, Agency for Science, Technology and Research, Singapore 138632 (e-mail: sunsm@ i2r.a-star.edu.sg).

transceivers, the authors in [6] theoretically proved that the mutualism relationship between the backscatter and primary links can be maintained and then maximized the weighted sum rate of all links for the scenario of a single backscatter link and that of multiple backscatter links, respectively. Integrating reconfigurable intelligent surface (RIS) with MSR, various resource allocation schemes have been designed to achieve a range of optimization objectives [8]–[14], including minimizing the PT's transmit power [8], [9], exploring the EE trade-off between the PT and the RIS [10], maximizing the system EE [11], enhancing the system's secrecy rate [12], minimizing the system power consumption [13], and maximizing the weighted sum throughput of both the primary and backscatter links [14]. To meet the massive access demands of IoT nodes, non-orthogonal multiple access was adopted in MSR networks and the weighted sum rate of all the links was maximized in [15].

In the aforementioned works on SR [4]–[15], long-packet communications (LPC) were considered under the assumption of infinite blocklength for both the primary and backscatter links. However, in most IoT applications, such as factory automation, intelligent transportation and smart grids, IoT nodes typically transmit short data packets characterized by finite blocklengths [16]. Since Shannon capacity cannot characterize the achievable rates for short-packet communications (SPC) [17], [18], the findings presented in [4]–[15], which are based on Shannon capacity, are not applicable to IoT scenarios involving SPC. SR with hybrid long and short packets, where the PT performs LPC while the IoT nodes backscatter short packets, has mainly been studied for PSR [19]–[22]. Although MSR with hybrid long and short packets was investigated in [23], where the system EE was maximized and the transmit power of the PT was minimized, the work in [23] has not addressed the following limitations:

- The impact of the error probability (EP) of each IoT node's SPC on the primary transmission has been ignored in [23]. According to the joint decoding scheme [24], errors in estimating the short-packet information will degrade the performance of the primary transmission. Therefore, the achievable rate of the primary transmission is affected by the EP of each IoT node.
- Only a single IoT node was considered in [23]. Consequently, resource allocation for multi-IoT-node MSR with hybrid long and short packets has not been investigated yet.

Different from [23], in this work, we investigate resource allocation for a multi-IoT-node MSR network with hybrid long and short packets, where the PT transmits its long-packet data to the CR, while multiple IoT nodes sequentially backscatter their short packets to the CR via BackCom. For the considered network, we derive a more accurate expression for the primary transmission rate considering the EP of each IoT node's SPC and then propose a scheme to maximize the weighted sum throughput of all IoT nodes based on the derived expression. Our main contributions are summarized as follows.

- Considering the EP of each IoT node's SPC, we derive a lower bound expression for the primary transmission rate. Specifically, following the joint decoding scheme, the decoding of the PT's information can be categorized into two cases depending on whether or not the short-packet information is estimated correctly. In the case of correct estimation, the backscatter link is regarded as a multipath component of the primary transmission; otherwise, it is treated as co-channel interference to the primary transmission. Based on the above analysis and using the total probability theorem, we obtain the lower bound expression of the primary transmission rate.
- We formulate an optimization problem to maximize the weighted sum throughput of all IoT nodes by jointly optimizing the short-packet blocklength, PRC and EP of each IoT node, subject to the constraints on the quality-of-service (QoS) requirement and the energy causality for each IoT node, as well as the throughput gain for the primary transmission[1]. To tackle the formulated non-convex problem, we employ the block coordinate descent (BCD) method to decompose it into two subproblems: one optimizes the EP of each IoT node given the remaining variables and the other optimizes the short-packet blocklength and PRC of each IoT node given the EPs of all IoT nodes. The former is proven to be convex, while the latter can be efficiently solved using a successive convex approximation (SCA) based iterative algorithm. Based on the above solutions, we propose an iterative resource allocation scheme that solves the two subproblems alternately in each iteration until convergence.
- Simulation results verify the quick convergence of the proposed iterative algorithms and show that our proposed resource allocation scheme is superior to the existing resource allocation scheme for LPC based multi-IoT-node MSR networks [6] in terms of the weighted sum throughput of all IoT nodes. Besides, we obtain three key insights into the resource allocation for multi-IoT-node MSR networks with hybrid long and short packets.

The remainder of this paper is organized as follows. Section II presents the system model for the multi-IoT-node MSR network with hybrid long and short packets and provides a lower bound expression for the primary transmission rate considering the EP of each IoT node's SPC. Section III maximizes the weighted sum throughput of all IoT nodes subject to the constraints on the throughput gain for the primary transmission, etc. Simulation results are presented in Section IV, with conclusions provided in Section V.

II. System Model

As shown in Fig. 1, we consider a multi-IoT-node MSR network with hybrid long and short packets, where a PT transmits its long-packet data to a CR, while K IoT nodes take turns to backscatter their short packets to the

[1] As shown in [17], the maximum transmission rate of SPC is affected by its EP. That is, the EP of SPC serves not only as a critical performance metric but also as a key optimization variable. By choosing a proper EP, in conjunction with other factors such as the transmit power and short-packet blocklength, the transmitter can determine its maximum transmission rate, thereby enabling the selection of the number of transmission bits, modulation scheme, and other related parameters. Consequently, the optimization of the EP in SPC has been widely investigated in the existing works on SPC [25]–[27].

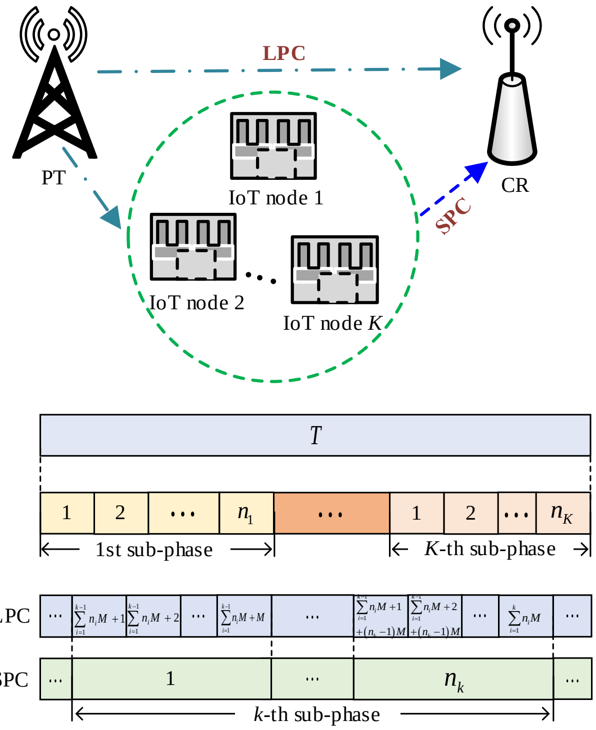

Fig. 1. System model.

CR via BackCom. Assume that all the devices are equipped with a single antenna. Following [23]–[26], we also assume that RF front ends for each transceiver are ideal. A block-fading channel model is considered, where all the channel coefficients remain unchanged within a transmission block and may vary across different transmission blocks. Let h_0, $h_{1,k}$, and $h_{2,k}, k \in \{1, 2, \ldots, K\}$ denote the channel gains of the PT−to−CR link, the PT−to−the k-th IoT node link, and the k-th IoT node−to−the CR link, respectively. We assume that all channel gains can be estimated perfectly at the beginning of each transmission block by means of existing channel estimation techniques [28]. Note that in real-world IoT systems, channel estimation errors and latency may exist, potentially degrading system performance. However, in this work, our focus is to quantify the upper bound performance of the PT and IoT nodes in MSR with the hybrid long and short packets under a given information transmission time budget, independently of the effects caused by imperfect channel estimation. Thus, we assume perfect channel state information (CSI) for all links as in existing works, such as [23]–[26], while optimizing the resource allocation under imperfect CSI is beyond the scope of this work.

Let x_{p} with $\mathbb{E}[|x_{\mathrm{p}}|^2] = 1$ denote the long-packet information symbol transmitted by the PT, where $\mathbb{E}[\cdot]$ represents the expectation operator. The duration of the given information transmission time budget within a transmission block is denoted by T and the number of channel uses within T is denoted by N. Then we have $T = NT_{\mathrm{p}}$, where T_{p} is the symbol period of x_{p}. During the primary transmission, K IoT nodes backscatter their short-packet information symbols, i.e., $x_{\mathrm{b},k}$ with $\mathbb{E}[|x_{\mathrm{b},k}|^2] = 1, \forall k$, to the CR in turn. Owing to the simple backscatter circuit at each IoT node and its low modulation rate, we consider that each IoT node's symbol period covers M ($M \gg 1$) primary symbol periods. Let T_{b} denote the symbol period of the short-packet symbol at each IoT node. Then we have $T_{\mathrm{b}} = MT_{\mathrm{p}}$. Besides, to avoid the co-channel interference among different IoT nodes, T is divided into K sub-phases, where the k-th IoT node only performs short-packet BackCom in the k-th sub-phase and harvests energy in the other sub-phases. Let n_k denote the short-packet blocklength of the k-th IoT node. Then we have $\sum_{k=1}^{K} n_k T_{\mathrm{b}} = \sum_{k=1}^{K} n_k M T_{\mathrm{p}} \leq T = NT_{\mathrm{p}}$.

A. Rate Analysis for Primary LPC

Let P_{t} denote the transmit power of the PT. Then in the k-th sub-phase, the received signal at the k-th IoT node is given by

$$y_{\mathrm{I},k} = \sqrt{P_{\mathrm{t}} h_{1,k}} x_{\mathrm{p}} + n_{\mathrm{I}}, \tag{1}$$

where $n_{\mathrm{I}} \sim \mathcal{CN}(0, \sigma^2)$ is the additive white Gaussian noise (AWGN) at the IoT node. Then the received signal will be partitioned into two parts according to its PRC, denoted by β_k. Specifically, $\sqrt{\beta_k} y_{\mathrm{I},k}$ is allocated for short-packet information backscattering and the remaining part is used for energy harvesting.

During the k-th sub-phase, the CR receives both the primary long-packet signal and backscattered short-packet signal from the k-th IoT node, and the received signal can be expressed as

$$y_{\mathrm{R},k} = \sqrt{P_{\mathrm{t}} h_0} x_{\mathrm{p}} + \sqrt{\beta_k P_{\mathrm{t}} h_{1,k} h_{2,k}} x_{\mathrm{p}} x_{\mathrm{b},k} + n_{\mathrm{R}}, \tag{2}$$

where $n_{\mathrm{R}} \sim \mathcal{CN}(0, \sigma^2)$ is the AWGN at the CR[2].

To successfully decode both x_{p} and $x_{\mathrm{b},k}$, we assume that the CR has a powerful computational capability, allowing it to conduct joint decoding to recover both x_{p} and $x_{\mathrm{b},k}$. According to the joint decoding scheme in [24], the CR should first decode x_{p} conditioned on each possible $x_{\mathrm{b},k}$, treating $\sqrt{\beta_k P_{\mathrm{t}} h_{1,k} h_{2,k}} x_{\mathrm{p}} x_{\mathrm{b},k}$ as a multipath component, and then obtain the estimation of x_{p} conditioned on $x_{\mathrm{b},k}$, denoted by $\widehat{x}_{\mathrm{p}}|_{x_{\mathrm{b},k}}$. Then by exploring all $\widehat{x}_{\mathrm{p}}|_{x_{\mathrm{b},k}}$, the estimation of $x_{\mathrm{b},k}$, denoted by $\widehat{x}_{\mathrm{b},k}$, is obtained with the minimal squared error. Finally, $\widehat{x}_{\mathrm{p}}|_{\widehat{x}_{\mathrm{b},k}}$ is used for decoding $x_{\mathrm{b},k}$. Specifically, based on $\widehat{x}_{\mathrm{p}}|_{\widehat{x}_{\mathrm{b},k}}$, the CR employs the successive interference cancellation (SIC) technique to eliminate $\sqrt{P_{\mathrm{t}} h_0} \widehat{x}_{\mathrm{p}}|_{\widehat{x}_{\mathrm{b},k}}$ from $y_{\mathrm{R},k}$ and then decodes $x_{\mathrm{b},k}$ from the remaining signal.

As previously shown in the joint decoding scheme [24], any error in estimating $x_{\mathrm{b},k}$ can adversely affect the performance of the primary transmission. Since SPC is inherently subject to a non-zero packet EP due to the finite blocklength, the achievable rate of the primary transmission is affected by the EP of the k-th IoT node's short-packet BackCom, denoted by $\varepsilon_k, \forall k$. In order to characterize this impact, we consider two cases

[2]In (2), n_{I} is neglected for the following reason. According to [29], the AWGN at the receiver consists of the AWGN from both the receiving antenna and the RF-to-baseband conversion, where the AWGN from the RF-to-baseband conversion is typically much larger than that from the receiving antenna. Since BackCom does not require RF-to-baseband conversion, n_{I} is solely determined by the AWGN from the receiving antenna, which is relatively small and can therefore be ignored.

for the decoding of x_{p}. In the case of successfully estimating $x_{\mathrm{b},k}$ with a probability of $1-\varepsilon_k$, $\sqrt{\beta_k P_{\mathrm{t}} h_{1,k} h_{2,k}} x_{\mathrm{p}} x_{\mathrm{b},k}$ can be deemed as x_{p} passing through a slowly varying channel $\sqrt{\beta_k P_{\mathrm{t}} h_{1,k} h_{2,k}} x_{\mathrm{b},k}$ due to the fact that $x_{\mathrm{b},k}$ remains constant over M long-packet symbol periods. Accordingly, the signal to noise ratio (SNR) for decoding x_{p} within the symbol period of $x_{\mathrm{b},k}$ is given by

$$\gamma_{\mathrm{p}}^{\mathrm{s}}\left(x_{\mathrm{b},k}\right)=\frac{P_{\mathrm{t}} h_0+\beta_k P_{\mathrm{t}} h_{1,k} h_{2,k}\left|x_{\mathrm{b},k}\right|^2}{\sigma^2}. \tag{3}$$

In the case of failed estimation of $x_{\mathrm{b},k}$ with a probability of ε_k, it is challenging to characterize the corresponding SNR. To facilitate analysis, in this case, we treat $\sqrt{\beta_k P_{\mathrm{t}} h_{1,k} h_{2,k}} x_{\mathrm{p}} x_{\mathrm{b},k}$ as the co-channel interference to obtain a lower bound of the primary transmission rate. Correspondingly, the decoding signal to interference plus noise ratio (SINR) of x_{p} is given by

$$\gamma_{\mathrm{p}}^{\mathrm{f}}\left(x_{\mathrm{b},k}\right)=\frac{P_{\mathrm{t}} h_0}{\beta_k P_{\mathrm{t}} h_{1,k} h_{2,k}\left|x_{\mathrm{b},k}\right|^2+\sigma^2}. \tag{4}$$

Using the total probability theorem, the lower bound expression of the primary transmission rate (bit/s/Hz) in the k-th sub-phase can be determined by

$$\begin{aligned} R_{\mathrm{p},k}= & \mathbb{E}_{x_{\mathrm{b},k}}\left[\left(1-\varepsilon_k\right) \log_2\left(1+\gamma_{\mathrm{p}}^{\mathrm{s}}\left(x_{\mathrm{b},k}\right)\right)\right. \\ & \left.+\varepsilon_k \log_2\left(1+\gamma_{\mathrm{p}}^{\mathrm{f}}\left(x_{\mathrm{b},k}\right)\right)\right]. \end{aligned} \tag{5}$$

Remark 1: If each IoT node performs LPC, i.e., $\varepsilon_k=0, \forall k$, the expression in (5) can be simplified to $\mathbb{E}_{x_{\mathrm{b},k}}\left[\log_2\left(1+\gamma_{\mathrm{p}}^{\mathrm{s}}\left(x_{\mathrm{b},k}\right)\right)\right]$, which aligns with Eq. (11) of [5]. This indicates that the achievable rate for the primary transmission in the LPC-based MSR network can be considered a special case of (5). In the case of $\varepsilon_k=1, \forall k$, i.e., the CR consistently fails to estimate $x_{\mathrm{b},k}$, $\sqrt{\beta_k P_{\mathrm{t}} h_{1,k} h_{2,k}} x_{\mathrm{p}} x_{\mathrm{b},k}$ does not enhance the primary transmission according to the joint decoding scheme. In this case, the achievable rate of the primary transmission can be approximated as $\mathbb{E}_{x_{\mathrm{b},k}}\left[\log_2\left(1+\gamma_{\mathrm{p}}^{\mathrm{f}}\left(x_{\mathrm{b},k}\right)\right)\right]$.

B. Rate Analysis for IoT Nodes' SPC

If the PT transmits long packets with the rate of $R_{\mathrm{p},k}$ in the k-th sub-phase, then its signal can be successfully decoded by the CR. After performing SIC to perfectly remove the interference caused by the primary transmission, the CR employs maximal ratio combining (MRC) across M consecutive LPC symbol periods to decode $x_{\mathrm{b},k}$ [5]. Then the corresponding SNR is given by

$$\gamma_k=\frac{M \beta_k P_{\mathrm{t}} h_{1,k} h_{2,k}}{\sigma^2}. \tag{6}$$

Then the corresponding rate (bit per short-packet blocklength) is determined as

$$R_{\mathrm{b},k}=\log_2\left(1+\gamma_k\right)-\sqrt{\frac{V\left(\gamma_k\right)}{n_k}} Q^{-1}\left(\varepsilon_k\right), \tag{7}$$

where $V\left(\gamma_k\right)=1-\left(1+\gamma_k\right)^{-2}$ denotes the channel dispersion, $Q^{-1}(\cdot)$ expresses the inverse Gaussian Q function, and $Q(x)=\int_x^{+\infty} \frac{e^{-\frac{t^2}{2}}}{\sqrt{2\pi}} dt$.

C. Total Harvested Energy at Each IoT Node

In order to maximize the total energy harvested at the k-th IoT node within T, we assume that the k-th IoT node can harvest energy not only during the k-th sub-phase but also across the other sub-phases. Consequently, the total harvested energy at the k-th IoT node can be calculated as

$$E_{\mathrm{h},k}=n_k T_{\mathrm{b}} \eta\left(1-\beta_k\right) P_{\mathrm{t}} h_{1,k}+\eta\left(T-n_k T_{\mathrm{b}}\right) P_{\mathrm{t}} h_{1,k}, \tag{8}$$

where η denotes the fixed energy conversion efficiency. From (8), we can observe that $E_{\mathrm{h},k}$ consists of two components. The first component, $n_k T_{\mathrm{b}} \eta\left(1-\beta_k\right) P_{\mathrm{t}} h_{1,k}$, corresponds to the energy harvested during the k-th sub-phase, while the second component, $\eta\left(T-n_k T_{\mathrm{b}}\right) P_{\mathrm{t}} h_{1,k}$, represents the energy harvested across the remaining sub-phases.

III. Weighted Sum Throughput Maximization

In order to enhance the performance of the IoT nodes' SPC, in this section, we address the maximization of the weighted sum throughput achieved by all IoT nodes for the considered network while ensuring the PT's throughput gain. In particular, we formulate the weighted sum throughput maximization problem by jointly optimizing the short-packet blocklength, PRC and EP of each IoT node. Since the formulated joint optimization problem is highly non-convex, we solve it by proposing efficient algorithms.

A. Problem Formulation

In this subsection, we first derive the expression of the weighted sum throughput of all IoT nodes and then introduce necessary constraints on the QoS requirement and energy causality for each IoT node, as well as the throughput gain for the primary transmission.

Following [26], the k-th IoT node's effective throughput can be determined by

$$C_{\mathrm{b},k}=\left(1-\varepsilon_k\right) n_k R_{\mathrm{b},k}. \tag{9}$$

Let w_k with $w_k \geq 0$ denote the weighting factor at the k-th IoT node, which indicates the k-th IoT node's priority in allocating wireless resources among all IoT nodes. Specifically, a larger w_k means that more resources may be allocated to the k-th IoT node. Accordingly, the weighted sum throughput of all IoT nodes can be expressed as

$$C_{\mathrm{ws}}=\sum\nolimits_{k=1}^K w_k C_{\mathrm{b},k}=\sum\nolimits_{k=1}^K w_k\left(1-\varepsilon_k\right) n_k R_{\mathrm{b},k}. \tag{10}$$

Likewise, based on (9), the QoS constraint for each IoT node can be represented as

$$C_{\mathrm{b},k}=\left(1-\varepsilon_k\right) n_k R_{\mathrm{b},k} \geq C_{\min,k}, \forall k, \tag{11}$$

where $C_{\min,k}$ denotes the minimum effective throughput required at the k-th IoT node.

In order to minimize the consumption of battery energy at each IoT node, we assume that each IoT node relies solely on its harvested energy to support BackCom. This approach allows for an extended operational time for each IoT node. Under this assumption, to facilitate short-packet BackCom for the IoT node, we further assume that the energy consumed for BackCom does not exceed the energy harvested by the IoT node. This assumption is valid since each IoT node can first utilize the energy stored in its battery and subsequently replenish any battery energy loss with the harvested energy [19]. Let $P_{\mathrm{c},k}$ denote the circuit power consumption for the k-th IoT node's BackCom. Then the energy-causality constraint for each IoT node is denoted by

$$P_{\mathrm{c},k} n_k T_{\mathrm{b}} \le E_{\mathrm{h},k}, \\ \Rightarrow P_{\mathrm{c},k} n_k \le \eta P_{\mathrm{t}} h_{1,k} \left(N_{\mathrm{s}} - n_k \beta_k\right), \forall k, \tag{12}$$

where $N_{\mathrm{s}} = \frac{N}{M}$.

As for the primary transmission, its lower bound throughput can be determined by

$$\begin{aligned} C_{\mathrm{p}} &= B \sum\nolimits_{k=1}^{K} n_k T_{\mathrm{b}} R_{\mathrm{p},k} + B\left(T - \sum\nolimits_{k=1}^{K} n_k T_{\mathrm{b}}\right) R_{\mathrm{p},0} \\ &= B T_{\mathrm{b}} \sum\nolimits_{k=1}^{K} n_k \mathbb{E}_{x_{\mathrm{b},k}}\left[(1-\varepsilon_k)\log_2\left(1+\gamma_{\mathrm{p}}^{\mathrm{s}}(x_{\mathrm{b},k})\right) + \varepsilon_k \right. \\ &\quad \left. \times \log_2\left(1+\gamma_{\mathrm{p}}^{\mathrm{f}}(x_{\mathrm{b},k})\right)\right] + B\left(T - \sum\nolimits_{k=1}^{K} n_k T_{\mathrm{b}}\right) R_{\mathrm{p},0}, \end{aligned} \tag{13}$$

where B is the system bandwidth, and $R_{\mathrm{p},0} = \log_2\left(1 + \frac{P_{\mathrm{t}} h_0}{\sigma^2}\right)$ denotes the achievable rate for the primary transmission when none of the IoT nodes engage in BackCom.

Note that for the primary transmission without any IoT nodes' BackCom, its throughput per transmission block is given by $BTR_{\mathrm{p},0}$. By comparing C_{p} with $BTR_{\mathrm{p},0}$, we can observe that the existence of the EP in each IoT node's BackCom may destroy the mutual benefits between the primary transmission and the IoT nodes' BackCom since the throughput gain for the primary transmission may not be always guaranteed. For example, with a larger ε_k, $\mathbb{E}_{x_{\mathrm{b},k}}\left[(1-\varepsilon_k)\log_2\left(1+\gamma_{\mathrm{p}}^{\mathrm{s}}(x_{\mathrm{b},k})\right) + \varepsilon_k \log_2\left(1+\gamma_{\mathrm{p}}^{\mathrm{f}}(x_{\mathrm{b},k})\right)\right]$ may be smaller than $R_{\mathrm{p},0}$. Consequently, it is plausible that the primary transmission throughput is less than $BTR_{\mathrm{p},0}$. Therefore, in order to guarantee a minimum throughput gain for the primary transmission, the following constraint should be included in the formulated problem,

$$\begin{aligned} &C_{\mathrm{p}} - BTR_{\mathrm{p},0} \ge \Delta \Rightarrow BT_{\mathrm{b}} \sum\nolimits_{k=1}^{K} n_k \big(\mathbb{E}_{x_{\mathrm{b},k}}[(1-\varepsilon_k)\log_2\big(1 \\ &+ \gamma_{\mathrm{p}}^{\mathrm{s}}(x_{\mathrm{b},k})\big) + \varepsilon_k \log_2\left(1+\gamma_{\mathrm{p}}^{\mathrm{f}}(x_{\mathrm{b},k})\right)] - R_{\mathrm{p},0}\big) \ge \Delta, \end{aligned} \tag{14}$$

where $\Delta > 0$ denotes the minimum throughput gain required for the primary transmission.

Based on (10), (11), (12) and (14), the weighted sum throughput maximization problem can be formulated as

$$\begin{aligned} \mathbf{P_0}: \max_{\boldsymbol{\beta},\mathbf{n},\boldsymbol{\varepsilon}} \quad & C_{\mathrm{ws}} \\ \text{s.t.}\ & \mathrm{C1}: (11), \\ & \mathrm{C2}: (12), \\ & \mathrm{C3}: (14), \\ & \mathrm{C4}: \sum\nolimits_{k=1}^{K} n_k \le \lfloor N_{\mathrm{s}} \rfloor, \\ & \mathrm{C5}: 0 \le \beta_k \le 1,\ \forall k, \\ & \mathrm{C6}: 0 \le \varepsilon_k \le \varepsilon_{\max}, \forall k, \\ & \mathrm{C7}: n_k \in \mathbb{Z}, \forall k, \end{aligned}$$

where $\boldsymbol{\beta} = [\beta_1, \ldots, \beta_K]$, $\mathbf{n} = [n_1, \ldots, n_K]$, $\boldsymbol{\varepsilon} = [\varepsilon_1, \ldots, \varepsilon_K]$, $\lfloor\cdot\rfloor$ represents the flooring operation, $\varepsilon_{\max}$ denotes the maximum tolerable EP at each IoT node, and $\mathbb{Z}$ represents the non-negative integer set.

In $\mathbf{P_0}$, C1 and C2 are the QoS and energy-causality constraints for each IoT node, respectively. C3 ensures the minimum throughput gain for the primary transmission. C4 constrains that all IoT nodes' short packets should be backscattered within T. C5 and C6 specify the maximum values of β_k and ε_k, respectively. C7 indicates that the short-packet blocklength of each IoT node should be a non-negative integer.

It can be observed that the non-convexities of $\mathbf{P_0}$ stem from three factors. Firstly, the intricacy inherent in $R_{\mathrm{b},k}$ amplifies the complexity of $C_{\mathrm{b},k}$, leading to a highly non-convex objective function and constraint C1. Specifically, $C_{\mathrm{b},k}$ not only involves the coupled relationships among β_k, n_k and $\varepsilon_k, \forall k$, but also includes several complicated functions, i.e., the logarithmic function, the inverse Gaussian Q function, etc. As a result, both the objective function and constraint C1 pose significant challenges in solving $\mathbf{P_0}$. Secondly, the impact of the EP of each IoT node's SPC on the primary transmission introduces a coupled relationship between ε_k and other variables, further complicating the expression for the primary transmission throughput C_{p}. This results in the highly non-convex nature of constraint C3, making it a major challenge in solving $\mathbf{P_0}$. Thirdly, the optimization of the integer variable $n_k, \forall k$ presents an additional challenge due to its high computational complexity.

B. Solution to $\mathbf{P_0}$

By means of several convex tools, we analyze the solution to $\mathbf{P_0}$. Specifically, Lemma 1 is provided to analyze the optimal n_k, denoted by $n_k^{\ddagger}, \forall k$.

Lemma 1: For the considered network, the weighted sum throughput of all IoT nodes is maximized under either of the two scenarios. In the first scenario, all IoT nodes engage in sequential short-packet BackCom throughout the given information transmission time budget T, i.e., $\sum_{k=1}^{K} n_k^{\ddagger} = \lfloor N_{\mathrm{s}} \rfloor$. In the second scenario, they exhaust or almost exhaust all their harvested energy for BackCom, i.e., $n_k^{\ddagger} = \lfloor \frac{N_{\mathrm{s}}}{B_k + \beta_k} \rfloor, \forall k$, where $B_k = \frac{P_{\mathrm{c},k}}{\eta P_{\mathrm{t}} h_{1,k}}$.

Proof. Please see Appendix A. ■

Remark 2: According to Lemma 1, we can observe that when $\sum_{k=1}^{K} \left\lfloor \frac{N_{\mathrm{s}}}{B_k+1} \right\rfloor > \lfloor N_{\mathrm{s}} \rfloor$ holds, we have $\sum_{k=1}^{K} \left\lfloor \frac{N_{\mathrm{s}}}{B_k+\beta_k} \right\rfloor > \lfloor N_{\mathrm{s}} \rfloor$ due to $\left\lfloor \frac{N_{\mathrm{s}}}{B_k+\beta_k} \right\rfloor \ge \left\lfloor \frac{N_{\mathrm{s}}}{B_k+1} \right\rfloor$. In this case, $n_k^{\ddagger}, \forall k$ is constrained by $\sum_{k=1}^{K} n_k^{\ddagger} = \lfloor N_{\mathrm{s}} \rfloor$. Note that achieving $\sum_{k=1}^{K} \left\lfloor \frac{N_{\mathrm{s}}}{B_k+1} \right\rfloor > \lfloor N_{\mathrm{s}} \rfloor$ is facilitated by selecting a small B_k, a condition achieved by either setting a small $P_{\mathrm{c},k}$ or a large $\eta P_{\mathrm{t}} h_{1,k}$. Likewise, for the case with $\sum_{k=1}^{K} \left\lfloor \frac{N_{\mathrm{s}}}{B_k} \right\rfloor < \lfloor N_{\mathrm{s}} \rfloor$, we obtain $\sum_{k=1}^{K} \left\lfloor \frac{N_{\mathrm{s}}}{B_k+\beta_k} \right\rfloor < \lfloor N_{\mathrm{s}} \rfloor$ owing to $\left\lfloor \frac{N_{\mathrm{s}}}{B_k+\beta_k} \right\rfloor < \left\lfloor \frac{N_{\mathrm{s}}}{B_k} \right\rfloor$. Correspondingly, $n_k^{\ddagger}$ is determined by $\lfloor \frac{N_{\mathrm{s}}}{B_k+\beta_k} \rfloor, \forall k$.

On this basis, we can reformulate $\mathbf{P_0}$ as

$$\begin{aligned}&\mathbf{P_1}: \max_{\boldsymbol{\beta},\mathbf{n},\boldsymbol{\varepsilon}} \quad C_{\rm ws}\\ &\text{s.t. C1, C3, C5, C6, C7},\\ &\text{C2}-1: \begin{cases} B_k n_k = N_{\rm s} - n_k\beta_k, \forall k, \\ \text{if} \sum_{k=1}^{K} \left\lfloor \frac{N_{\rm s}}{B_k} \right\rfloor < \lfloor N_{\rm s} \rfloor \text{ is met} \\ B_k n_k \leq N_{\rm s} - n_k\beta_k, \forall k, \text{otherwise} \end{cases},\\ &\text{C4}-1: \begin{cases} \sum_{k=1}^{K} n_k = \lfloor N_{\rm s} \rfloor, \\ \text{if} \sum_{k=1}^{K} \left\lfloor \frac{N_{\rm s}}{B_k+1} \right\rfloor > \lfloor N_{\rm s} \rfloor \text{ holds} \\ \sum_{k=1}^{K} n_k \leq \lfloor N_{\rm s} \rfloor, \text{otherwise} \end{cases}.\end{aligned}$$

Although $\mathbf{P_1}$ is more tractable than $\mathbf{P_0}$, it is still difficult to solve since the coupled relationship between $\boldsymbol{\varepsilon}$ and other variables still exists. To address this issue, the conventional approach is to employ an exhaustive search method. Although this approach guarantees finding the optimal solution, it is characterized by high computational complexity. To solve $\mathbf{P_1}$ with low computational complexity, we utilize the BCD method to obtain a locally optimal (near-optimal) solution. Specifically, we decompose $\mathbf{P_1}$ into two subproblems, denoted by $\mathbf{P_{1a}}$ and $\mathbf{P_{1b}}$. In $\mathbf{P_{1a}}$, $\boldsymbol{\varepsilon}$ is optimized to maximize the weighted sum throughput of all IoT nodes under given $\boldsymbol{\beta}$ and $\mathbf{n}$, while with given $\boldsymbol{\varepsilon}$, the weighted sum throughput is maximized by jointly optimizing $\boldsymbol{\beta}$ and $\mathbf{n}$ in $\mathbf{P_{1b}}$. Accordingly, the main challenge for solving $\mathbf{P_1}$ is how to tackle these two subproblems.

1) Solution to $\mathbf{P_{1a}}$: $\mathbf{P_{1a}}$ can be written as

$$\begin{aligned}&\mathbf{P_{1a}}: \max_{\boldsymbol{\varepsilon}} \quad C_{\rm ws}\\ &\text{s.t. C1, C3, C6.}\end{aligned}$$

Proposition 1: Given $\boldsymbol{\beta}$ and $\mathbf{n}$, it can be proven that $C_{\rm ws}$ is concave with respect to $\boldsymbol{\varepsilon}$, resulting in a convex optimization problem for $\mathbf{P_{1a}}$.

Proof. Please see Appendix B. ■

Although $\mathbf{P_{1a}}$ is proven to be convex, it cannot be solved via CVX directly due to the complicated Gaussian Q function in $C_{{\rm b},k}$. In what follows, we analyze the optimal solution to $\mathbf{P_{1a}}$ by means of convex tools. Let $\varepsilon_k^+, \forall k$ denote the optimal ε_k that maximizes $C_{\rm ws}$ while satisfying C6. Denote $\frac{\partial C_{\rm ws}}{\partial \varepsilon_k}$ by $F_k(\varepsilon_k)$. Then we have $F_k(\varepsilon_k) = \frac{\partial C_{\rm ws}}{\partial \varepsilon_k} = D_k Q^{-1}(\varepsilon_k) - (1-\varepsilon_k) D_k \frac{\partial Q^{-1}(\varepsilon_k)}{\partial \varepsilon_k} - C_k$, where $C_k = n_k w_k \log_2(1+\gamma_k)$ and $D_k = w_k\sqrt{n_k V(\gamma_k)}, \forall k$. When $F_k(\varepsilon_{\max}) \geq 0$ is satisfied, we obtain $F_k(\varepsilon_k) \geq F_k(\varepsilon_{\max}) \geq 0$ due to $\frac{\partial^2 C_{\rm ws}}{\partial \varepsilon_k^2} < 0$ as presented in (B.2). That is, $C_{\rm ws}$ is monotonically increasing with ε_k. Accordingly, ε_k^+ of this case is given by $\varepsilon_{\max}$. For the case with $F_k(\varepsilon_{\max}) < 0$, ε_k^+ is achieved by solving $F_k(\varepsilon_k) = 0$ when ε_k ranges from 0 to $\varepsilon_{\max}$. Based on $\frac{\partial^2 C_{\rm ws}}{\partial \varepsilon_k^2} < 0$, $F_k(\varepsilon_k)$ is monotonically decreasing with ε_k and $F_k(\varepsilon_k) = 0$ can be solved by using the bisection method. Correspondingly, ε_k^+ is given by

$$\varepsilon_k^+ = \begin{cases} \varepsilon_{\max}, \text{ if } F_k(\varepsilon_{\max}) \geq 0 \text{ is met}, \\ F_k^{-1}(0), \text{ otherwise}, \end{cases} \tag{15}$$

where $F_k^{-1}(\cdot)$ is the inverse function of $F_k(\varepsilon_k)$. Since $F_k(\varepsilon_k)$ is monotonically decreasing with ε_k, $F_k^{-1}(0)$ can be solved by using the bisection method.

Based on $\varepsilon_k^+, \forall k$, we can obtain the maximum throughput of each IoT node under C6, given by $C_{{\rm b},k}\big|_{\varepsilon_k=\varepsilon_k^+}$. If $C_{{\rm b},k}\big|_{\varepsilon_k=\varepsilon_k^+} \geq C_{\min,k}, \forall k$ holds, then there exists ε_k that satisfies $C_{{\rm b},k} = C_{\min,k}, \forall k$. Otherwise, $\mathbf{P_{1a}}$ is infeasible. Let $\varepsilon_k^\diamond$ be the solution to $C_{{\rm b},k} = C_{\min,k}, \forall k$ within $\varepsilon_k \in [0, \varepsilon_k^+]$. Then there are two cases for $\varepsilon_k^\diamond$. In the case with $C_{{\rm b},k}\big|_{\varepsilon_k=\varepsilon_k^+} = C_{\min,k}$, $\varepsilon_k^\diamond$ is determined by ε_k^+. For the case with $C_{{\rm b},k}\big|_{\varepsilon_k=\varepsilon_k^+} > C_{\min,k}$, the bisection method is adopted to obtain $\varepsilon_k^\diamond$.

Considering the monotonically decreasing behavior of $C_{\rm p}$ with respect to ε_k, we achieve that $\mathbf{P_{1a}}$ is infeasible when $C_{\rm p}|_{\varepsilon_k=\varepsilon_k^\diamond,\forall k} - BTR_{{\rm p},0} < \Delta$ holds. With $C_{\rm p}|_{\varepsilon_k=\varepsilon_k^\diamond,\forall k} - BTR_{{\rm p},0} \geq \Delta$ satisfied, $\mathbf{P_{1a}}$ can be transformed into

$$\begin{aligned}&\mathbf{P_{2a}}: \max_{\boldsymbol{\varepsilon}} \quad C_{\rm ws}\\ &\text{s.t. C3, C8}: \varepsilon_k^\diamond \leq \varepsilon_k \leq \varepsilon_k^+, \forall k.\end{aligned}$$

Under the range of $\varepsilon_k^\diamond \leq \varepsilon_k \leq \varepsilon_k^+, \forall k$, $C_{\rm ws}$ always increases with ε_k. Then the optimal ε_k to $\mathbf{P_{2a}}$, denoted by ε_k^*, is given by the upper bound of ε_k by combining C3 and C8. Specifically, if $C_{\rm p}|_{\varepsilon_k=\varepsilon_k^\diamond,\forall k} - BTR_{{\rm p},0} = \Delta$ is met, $\varepsilon_k^* = \varepsilon_k^\diamond, \forall k$ is achieved. For the case with $C_{\rm p}|_{\varepsilon_k=\varepsilon_k^+,\forall k} - BTR_{{\rm p},0} \geq \Delta$, we have $\varepsilon_k^* = \varepsilon_k^+, \forall k$. With $\left(C_{\rm p}|_{\varepsilon_k=\varepsilon_k^\diamond,\forall k} - BTR_{{\rm p},0} - \Delta\right)\left(C_{\rm p}|_{\varepsilon_k=\varepsilon_k^+,\forall k} - BTR_{{\rm p},0} - \Delta\right) < 0$ satisfied, the values of ε_k^* for all k should satisfy $C_{\rm p}\big|_{\varepsilon_k=\varepsilon_k^*,\forall k} - BTR_{{\rm p},0} = \Delta$. In order to achieve ε_k^* of this case, the Lagrange duality method is employed, resulting in the following proposition.

Proposition 2: Given the non-negative Lagrange multiplier θ, the optimal ε_k to $\mathbf{P_{2a}}$ under the case with $\left(C_{\rm p}|_{\varepsilon_k=\varepsilon_k^\diamond} - BTR_{{\rm p},0} - \Delta\right)\left(C_{\rm p}|_{\varepsilon_k=\varepsilon_k^+} - BTR_{{\rm p},0} - \Delta\right) < 0$ is given by

$$\varepsilon_k^* = \begin{cases} \varepsilon_k^\diamond, \text{if } \theta\omega_k \geq F_k(\varepsilon_k^\diamond), \\ F_k^{-1}(\theta\omega_k), \text{if } F_k(\varepsilon_k^\diamond) < \theta\omega_k < F_k(\varepsilon_k^+), \\ \varepsilon_k^+, \text{if } \theta\omega_k \leq F_k(\varepsilon_k^+), \end{cases} \tag{16}$$

where $\omega_k = BT_{\rm b} n_k \mathbb{E}_{x_{{\rm b},k}}\!\left[\log_2\!\left(1+\gamma_{\rm p}^{\rm s}(x_{{\rm b},k})\right) - \log_2\!\left(1+\gamma_{\rm p}^{\rm f}(x_{{\rm b},k})\right)\right]$ and θ is updated following [30].

Proof. Please see Appendix C. ■

2) Solution to $\mathbf{P_{1b}}$: $\mathbf{P_{1b}}$ can be expressed as

$$\begin{aligned}&\mathbf{P_{1b}}: \max_{\boldsymbol{\beta},\mathbf{n}} \quad C_{\rm ws}\\ &\text{s.t. C1, C2}-1\text{, C3, C4}-1\text{, C5, C7.}\end{aligned}$$

To tackle the mixed integer optimization problem in $\mathbf{P_{1b}}$, we first relax the integer variable n_k to a continuous one and then introduce the auxiliary variable $x_k = \beta_k n_k$ for all k, transforming $\mathbf{P_{1b}}$ into $\mathbf{P_{2b}}$. Then we aim to solve $\mathbf{P_{2b}}$ and obtain its solution. Since its obtained $\{n_k\}_{k=1}^K$ may not be the integer set, which could potentially violate constraint C7 in $\mathbf{P_{1b}}$, we need to convert the obtained $\{n_k\}_{k=1}^K$ into the integer set, achieving the solution to $\mathbf{P_{1b}}$. In what follows, we focus on how to solve $\mathbf{P_{2b}}$, which is given by

$$\begin{aligned}\mathbf{P_{2b}}: \max_{\mathbf{x},\mathbf{n}} \quad & \sum_{k=1}^{K} A_k\left(R_k^{(1)}(x_k,n_k)-R_k^{(2)}(x_k,n_k)\right)\\ \text{s.t. } & \mathrm{C1}-1: R_k^{(1)}(x_k,n_k)-R_k^{(2)}(x_k,n_k)\ge \tfrac{C_{\min,k}}{1-\varepsilon_k},\forall k,\\ & \mathrm{C2}-2: \begin{cases} B_k n_k = N_{\mathrm{s}}-x_k,\forall k, \\ \text{if } \sum_{k=1}^{K}\left\lfloor \frac{N_{\mathrm{s}}}{B_k}\right\rfloor < \lfloor N_{\mathrm{s}}\rfloor \text{ is met} \\ B_k n_k \le N_{\mathrm{s}}-x_k,\forall k,\text{otherwise}\end{cases},\\ & \mathrm{C3}-1: B\sum_{k=1}^{K}(C'_{\mathrm{p},k}-n_k R_{\mathrm{p},0})T_{\mathrm{b}}\ge\Delta, \mathrm{C4}-1,\\ & \mathrm{C5}-1: 0\le x_k\le n_k,\forall k, \mathrm{C7}-1: n_k\ge 0,\forall k,\end{aligned}$$

where $A_k = w_k(1-\varepsilon_k)$, $R_k^{(1)}(x_k,n_k) = n_k\log_2\left(1+\frac{a_k x_k}{n_k}\right)$ with $a_k = \frac{MP_{\mathrm{t}}h_{1,k}h_{2,k}}{\sigma^2}$, $R_k^{(2)}(x_k,n_k) = \sqrt{n_k V\left(\frac{a_k x_k}{n_k}\right)}Q^{-1}(\varepsilon_k)$ and $C'_{\mathrm{p},k} = n_k\mathbb{E}_{x_{\mathrm{b},k}}\left[\log_2\left(1+\frac{P_{\mathrm{t}}h_0}{\sigma^2}+\frac{x_k b_k}{n_k}\right)-\varepsilon_k\log_2\left(1+\frac{x_k b_k}{n_k}\right)\right]$ with $b_k = \frac{P_{\mathrm{t}}h_{1,k}h_{2,k}|x_{\mathrm{b},k}|^2}{\sigma^2}$. It is important to highlight that the terms $R_k^{(1)}(x_k,n_k)$ and $R_k^{(2)}(x_k,n_k)$ represent distinct components of the achievable throughput for the k-th IoT node, namely $n_k R_{\mathrm{b},k}$, while $C'_{\mathrm{p},k}$ denotes a component of the throughput of the primary transmission C_{p}.

Proposition 3: $\mathbf{P_{2b}}$ is still non-convex due to the difference of two concave functions existing in both the objective function and constraints, such as $\mathrm{C1}-1$ and $\mathrm{C3}-1$.

Proof. Please see Appendix D. ■

According to Proposition 3, the concave functions $R_k^{(2)}(x_k,n_k)$ and $\mathbb{E}_{x_{\mathrm{b},k}}\left[n_k\varepsilon_k\log_2\left(1+\frac{x_k b_k}{n_k}\right)\right]$ in $C'_{\mathrm{p},k}$ lead to the non-convexity of $\mathbf{P_{2b}}$. To tackle it, following [31]–[33], the SCA method is employed, where we replace $R_k^{(2)}(x_k,n_k)$ and $\mathbb{E}_{x_{\mathrm{b},k}}\left[n_k\varepsilon_k\log_2\left(1+\frac{x_k b_k}{n_k}\right)\right]$ with their first-order Taylor expansions, bringing a lower bound for $\mathbf{P_{2b}}$. Then the locally optimal (near-optimal) solution to $\mathbf{P_{2b}}$ can be obtained by optimizing the lower bound of $\mathbf{P_{2b}}$ iteratively.

Let $n_k^{(0)}$ and $x_k^{(0)},\forall k$ denote the initial n_k and $x_k,\forall k$. Then we have

$$\begin{aligned}R_k^{(2)}(x_k,n_k) &\le R_k^{\mathrm{up}}\left(x_k^{(0)},n_k^{(0)},x_k,n_k\right) = R_k^{(2)}\left(x_k^{(0)},n_k^{(0)}\right)\\ &+D_k^{(1)}\left(x_k^{(0)},n_k^{(0)}\right)\left(x_k-x_k^{(0)}\right)+D_k^{(2)}\left(x_k^{(0)},n_k^{(0)}\right)\left(n_k-n_k^{(0)}\right),\end{aligned} \tag{17}$$

where $D_k^{(1)}\left(x_k^{(0)},n_k^{(0)}\right)$ and $D_k^{(2)}\left(x_k^{(0)},n_k^{(0)}\right)$ are the first-order derivatives of $R_k^{(2)}(x_k,n_k)$ with respect to x_k and n_k while letting $x_k = x_k^{(0)}$ and $n_k = n_k^{(0)}$.

Based on the expression of $R_k^{(2)}(x_k,n_k)$, we can derive $D_k^{(1)}\left(x_k^{(0)},n_k^{(0)}\right)$ and $D_k^{(2)}\left(x_k^{(0)},n_k^{(0)}\right)$ as

$$\begin{aligned}D_k^{(1)}\left(x_k^{(0)},n_k^{(0)}\right) &= \frac{\partial R_k^{(2)}(x_k,n_k)}{\partial x_k}\Big|_{x_k=x_k^{(0)},n_k=n_k^{(0)}}\\ &= \frac{a_k\left(n_k^{(0)}\right)^{\frac{5}{2}}\left(V\left(\frac{a_k x_k^{(0)}}{n_k^{(0)}}\right)\right)^{-\frac{1}{2}}Q^{-1}(\varepsilon_k)}{\left(n_k^{(0)}+a_k x_k^{(0)}\right)^3},\end{aligned} \tag{18}$$

$$\begin{aligned}D_k^{(2)}\left(x_k^{(0)},n_k^{(0)}\right) &= \frac{\partial R_k^{(2)}(x_k,n_k)}{\partial n_k}\Big|_{x_k=x_k^{(0)},n_k=n_k^{(0)}} = \frac{1}{2}\left(n_k^{(0)}\right)^{-\frac{1}{2}}\\ &\times\left(V\left(\frac{a_k x_k^{(0)}}{n_k^{(0)}}\right)\right)^{\frac{1}{2}}Q^{-1}(\varepsilon_k)-\frac{D_k^{(1)}\left(x_k^{(0)},n_k^{(0)}\right)x_k^{(0)}}{n_k^{(0)}}.\end{aligned} \tag{19}$$

Likewise, we can obtain the upper bound of $\mathbb{E}_{x_{\mathrm{b},k}}\left[n_k\varepsilon_k\log_2\left(1+\frac{x_k b_k}{n_k}\right)\right]$ as

$$\begin{aligned}&\mathbb{E}_{x_{\mathrm{b},k}}\left[n_k\varepsilon_k\log_2\left(1+\frac{x_k b_k}{n_k}\right)\right]\le C_k^{\mathrm{up}}\left(x_k^{(0)},n_k^{(0)},x_k,n_k\right)\\ &=\mathbb{E}_{x_{\mathrm{b},k}}\left[n_k^{(0)}\varepsilon_k\log_2\left(1+\frac{x_k^{(0)}b_k}{n_k^{(0)}}\right)\right]+D_k^{(3)}\left(x_k^{(0)},n_k^{(0)}\right)\\ &\times\left(x_k-x_k^{(0)}\right)+D_k^{(4)}\left(x_k^{(0)},n_k^{(0)}\right)\left(n_k-n_k^{(0)}\right),\end{aligned} \tag{20}$$

where $D_k^{(3)}\left(x_k^{(0)},n_k^{(0)}\right)$ and $D_k^{(4)}\left(x_k^{(0)},n_k^{(0)}\right)$ are the first-order derivatives of $\mathbb{E}_{x_{\mathrm{b},k}}\left[n_k\varepsilon_k\log_2\left(1+\frac{x_k b_k}{n_k}\right)\right]$ with respect to x_k and n_k while letting $x_k = x_k^{(0)}$ and $n_k = n_k^{(0)}$, given by

$$D_k^{(3)}\left(x_k^{(0)},n_k^{(0)}\right) = \mathbb{E}_{x_{\mathrm{b},k}}\left[\frac{b_k n_k^{(0)}\varepsilon_k}{\left(n_k^{(0)}+x_k^{(0)}b_k\right)\ln 2}\right], \tag{21}$$

$$\begin{aligned}&D_k^{(4)}\left(x_k^{(0)},n_k^{(0)}\right)\\ &=\mathbb{E}_{x_{\mathrm{b},k}}\left[\varepsilon_k\log_2\left(1+\frac{x_k^{(0)}b_k}{n_k^{(0)}}\right)-\frac{x_k^{(0)}b_k\varepsilon_k}{\left(n_k^{(0)}+x_k^{(0)}b_k\right)\ln 2}\right].\end{aligned} \tag{22}$$

Based on (17) and (20), the lower bound of $\mathbf{P_{2b}}$ under given $n_k^{(0)}$ and $x_k^{(0)},\forall k$ can be obtained as

$$\begin{aligned}\mathbf{P_{3b}}: \max_{\mathbf{x},\mathbf{n}} \quad & \sum_{k=1}^{K} A_k R_k^{\mathrm{low}}\\ \text{s.t. } & \mathrm{C1}-2: R_k^{\mathrm{low}}\ge\tfrac{C_{\min,k}}{1-\varepsilon_k},\forall k,\\ & \mathrm{C3}-2: B\sum_{k=1}^{K}(C_k^{\mathrm{low}}-n_k R_{\mathrm{p},0})T_{\mathrm{b}}\ge\Delta,\\ & \mathrm{C2}-2, \mathrm{C4}-1, \mathrm{C5}-1, \mathrm{C7}-1,\end{aligned}$$

where $R_k^{\mathrm{low}} = R_k^{(1)}(x_k,n_k) - R_k^{\mathrm{up}}\left(x_k^{(0)},n_k^{(0)},x_k,n_k\right)$ and $C_k^{\mathrm{low}} = n_k\mathbb{E}_{x_{\mathrm{b},k}}\left[\log_2\left(1+\frac{P_{\mathrm{t}}h_0}{\sigma^2}+\frac{x_k b_k}{n_k}\right)\right] - C_k^{\mathrm{up}}\left(x_k^{(0)},n_k^{(0)},x_k,n_k\right)$.

It can be observed that $\mathbf{P_{3b}}$ is convex and can be efficiently solved using the existing convex tools. On this basis, $\mathbf{P_{2b}}$ can be solved by optimally solving $\mathbf{P_{3b}}$ in each iteration until convergence. Let $\{n_k^{\triangle}\}$ and $\{\beta_k^{\triangle}\}$ denote the solution to $\mathbf{P_{2b}}$. Since the values of $n_k^{\triangle}$ for all k may not be integers, this leads to the violation of constraint C7 in $\mathbf{P_{1b}}$. Therefore, it is necessary to convert $n_k^{\triangle}$ to integers. A commonly used approach for this integer conversion is to round each $n_k^{\triangle}$ to the nearest integer, obtaining the integer solution, denoted by $\{n_k^*\}$. Then we need to verify whether $\{n_k^*\}$ satisfies all constraints of $\mathbf{P_{1b}}$. If all constraints are satisfied, then $\{n_k^*\}$ is considered the integer solution to $\mathbf{P_{1b}}$. However, it is important to note that not all constraints may be satisfied in this case. If any constraint is violated, a new integer conversion method must be developed to transform $n_k^{\triangle},\forall k$ into integer values while ensuring that all constraints are satisfied. The procedure for this proposed integer conversion method is outlined below.

3) Integer conversion for $\{n_k^{\triangle}\}$: According to Lemma 1, there are two cases for the value of $n_k^*, \forall k$. In the case where $n_k^{\triangle} = \frac{N_{\rm s}}{B_k+\beta_k^{\triangle}}$ holds for each k, if the set $\left\{\left\lfloor \frac{N_{\rm s}}{B_k+\beta_k^{\triangle}} \right\rfloor, \forall k\right\}$ meets constraints C1 and C3, then we output n_k^* as $n_k^* = \left\lfloor \frac{N_{\rm s}}{B_k+\beta_k^{\triangle}} \right\rfloor$ for all k. If not, $\mathbf{P_{1b}}$ is deemed infeasible. In the case where there exists at least one $n_k^{\triangle}$ that does not satisfy the equation $n_k^{\triangle} = \frac{N_{\rm s}}{B_k+\beta_k^{\triangle}}$, $\sum_{k=1}^{K} n_k^* = \lfloor N_{\rm s} \rfloor$ is required. Then n_k^* is decided by either $\left\lfloor n_k^{\triangle} \right\rfloor$ or $\left\lfloor n_k^{\triangle} \right\rfloor + 1$. To address it, we present the following three steps to determine n_k^* for all k.

Step 1: For the k-th IoT node, initially set $n_k^* = \left\lfloor n_k^{\triangle} \right\rfloor$ and verify whether $\{n_k^*\}$ satisfies constraints C1 and C$2-1$. If these constraints are not satisfied, update n_k^* as $\left\lfloor n_k^{\triangle} \right\rfloor + 1$ and repeat the verification process. If the constraints remain unsatisfied after this adjustment, then $\mathbf{P_{1b}}$ is considered infeasible. If $\mathbf{P_{1b}}$ remains feasible by repeating this process for k ranging from 1 to K, proceed to Step 2.

Step 2: If $\sum_{k=1}^{K} n_k^* > \lfloor N_{\rm s} \rfloor$, then $\mathbf{P_{1b}}$ is deemed infeasible. In the case where $\sum_{k=1}^{K} n_k^* = \lfloor N_{\rm s} \rfloor$, further verify if constraint C3 is satisfied. If constraint C3 is not satisfied, $\mathbf{P_{1b}}$ is considered infeasible. Otherwise, $\{n_k^*\}$ is considered a valid solution to $\mathbf{P_{1b}}$. If $\sum_{k=1}^{K} n_k^* < \lfloor N_{\rm s} \rfloor$, proceed to Step 3.

Step 3: Initially compute the remaining blocklength to be allocated as $N_{\rm r} = \lfloor N_{\rm s} \rfloor - \sum_{k=1}^{K} n_k^*$. This remaining blocklength can only be allocated to the k-th IoT node that satisfies $n_k^* = \left\lfloor n_k^{\triangle} \right\rfloor, \forall k$. It is worth noting that multiple IoT nodes may satisfy the aforementioned condition. In this case, for each potential IoT node, such as the k-th IoT node, we set $n_k^* = n_k^* + 1$ and evaluate whether the updated set $\{n_k^*\}$ meets all constraints of $\mathbf{P_{1b}}$. If all constraints are satisfied, then compute the weighted sum throughput of all IoT nodes as $C_k^{\rm r}$ and then revert n_k^* to its previous value by decrementing it by 1. Otherwise, set $C_k^{\rm r} = 0$ and revert n_k^* to its previous value. Subsequently, allocate this remaining blocklength to the IoT node with the maximum sum throughput. Update $\{n_k^*\}$ accordingly and decrement $N_{\rm r}$ by 1. This process continues until $N_{\rm r}$ reaches 0.

It is important to note that the proposed integer conversion method is applied only when rounding $n_k^{\triangle}$ is not feasible. Furthermore, Lemma 1 is utilized in the proposed method to efficiently determine n_k^* for all k, thereby reducing the overall complexity of the process.

C. Iterative Algorithms

In this subsection, we propose an efficient iterative algorithm to obtain the solution to $\mathbf{P_1}$, denoted by $\{\{n_k^{\rm o}\}, \{\beta_k^{\rm o}\}, \{\varepsilon_k^{\rm o}\}\}$. As has been mentioned in Section III-B, in order to solve $\mathbf{P_1}$, we should first solve its subproblems, namely $\mathbf{P_{1a}}$ and $\mathbf{P_{1b}}$. As for $\mathbf{P_{1a}}$, based on our analysis in Section III-B, if $\mathbf{P_{1a}}$ is feasible, there are three cases for the values of ε_k^* for all k. For the case with $C_{{\rm b},k}\big|_{\varepsilon_k=\varepsilon_k^+} \geq C_{\min,k}, \forall k$ and $C_{\rm p}|_{\varepsilon_k=\varepsilon_k^{\diamond}, \forall k} - BTR_{{\rm p},0} = \Delta$, ε_k^* is set as $\varepsilon_k^{\diamond}$ for each k. For the case with $C_{{\rm b},k}\big|_{\varepsilon_k=\varepsilon_k^+} \geq C_{\min,k}, \forall k$ and $C_{\rm p}|_{\varepsilon_k=\varepsilon_k^+, \forall k} - BTR_{{\rm p},0} \geq \Delta$, ε_k^* is given by ε_k^+ for all k. For the case with $C_{{\rm b},k}\big|_{\varepsilon_k=\varepsilon_k^+} \geq C_{\min,k}, \forall k$ and $\left(C_{\rm p}|_{\varepsilon_k=\varepsilon_k^{\diamond}, \forall k} - BTR_{{\rm p},0} - \Delta\right)\left(C_{\rm p}|_{\varepsilon_k=\varepsilon_k^+, \forall k} - BTR_{{\rm p},0} - \Delta\right) < 0$, we compute $\varepsilon_k^*, \forall k$ with given θ based on (16) and update θ using the gradient method [30] until θ achieves a convergent state. As for $\mathbf{P_{1b}}$, according to the SCA method and the proposed integer conversion method, Algorithm 1 is provided to obtain its solution.

Based on the solutions to $\mathbf{P_{1a}}$ and $\mathbf{P_{1b}}$, the iterative algorithm for solving $\mathbf{P_1}$ is presented in Algorithm 2 by leveraging the BCD method.

Algorithm 1 SCA based iterative algorithm for solving $\mathbf{P_{1b}}$

Set the maximum error tolerance as ϵ_0 and the initial values for $\{n_k\}$ and $\{\beta_k\}$ as $\{n_k^{(0)}\}$ and $\{\beta_k^{(0)}\}$;
Compute the initial value of $\{x_k\}$ as $x_k^{(0)} = n_k^{(0)}\beta_k^{(0)}, \forall k$ and set Flag $= 0$;
Set the initial value of $C_{\rm ws}$ as $C_{\rm ws}^{(0)} = 0$;
repeat
  Optimally solve $\mathbf{P_{3b}}$ with given $n_k^{(0)}$ and $x_k^{(0)}, \forall k$ via CVX and obtain the optimal solution as $n_k^{\dagger}$ and $x_k^{\dagger}, \forall k$;
  Compute the maximum sum throughput of all IoT nodes as $C_{\rm ws}^{\dagger} = \sum_{k=1}^{K} A_k R_k^{\rm low}\left(x_k^{\dagger}, n_k^{\dagger}\right)$;
  if $\left|C_{\rm ws}^{\dagger} - C_{\rm ws}^{(0)}\right| < \epsilon_0$ **then**
    Set $n_k^{\triangle} = n_k^{\dagger}$ and $\beta_k^{\triangle} = \frac{x_k^{\dagger}}{n_k^{\dagger}}, \forall k$;
    if $\{n_k^{\triangle}\}$ is an integer set **then**
      Set $n_k^* = n_k^{\triangle}$ for all k and Flag $= 1$;
    else
      $\{n_k^*\}$ is achieved by rounding each $n_k^{\triangle}$ to the nearest integer and set Flag $= 1$;
      if $\{n_k^*\}$ cannot satisfy all constrains of $\mathbf{P_{1b}}$ **then**
        $\{n_k^*\}$ is obtained by using the proposed integer conversion method;
      end if
    end if
  else
    Set $n_k^{(0)} = n_k^{\dagger}$, $x_k^{(0)} = x_k^{\dagger}, \forall k$ and $C_{\rm ws}^{(0)} = C_{\rm ws}^{\dagger}$;
  end if
until Flag $= 1$

---

1) Algorithm 1 for solving $\mathbf{P_{1b}}$: As shown in Algorithm 1, we set the initial values for $\{n_k\}$ and $\{\beta_k\}$ as $\{n_k^{(0)}\}$ and $\{\beta_k^{(0)}\}$ and the initial value of $C_{\rm ws}$ as $C_{\rm ws}^{(0)} = 0$. Given $n_k^{(0)}$ and $x_k^{(0)}, \forall k$, we optimally solve $\mathbf{P_{3b}}$ using CVX in each iteration, yielding the solution as $n_k^{\dagger}$ and $x_k^{\dagger}, \forall k$. Based on this solution, we can compute the corresponding weighted sum throughput as $C_{\rm ws}^{\dagger} = \sum_{k=1}^{K} A_k R_k^{\rm low}\left(x_k^{\dagger}, n_k^{\dagger}\right)$. If the stopping condition, i.e., $\left|C_{\rm ws}^{\dagger} - C_{\rm ws}^{(0)}\right| < \epsilon_0$, is met, then we set the solution to $\mathbf{P_{2b}}$, namely $\{n_k^{\triangle}\}$ and $\{\beta_k^{\triangle}\}$, as $n_k^{\triangle} = n_k^{\dagger}$ and $\beta_k^{\triangle} = \frac{x_k^{\dagger}}{n_k^{\dagger}}, \forall k$, where ϵ_0 denotes the maximum error tolerance. Otherwise, $n_k^{(0)}$, $x_k^{(0)}, \forall k$ and $C_{\rm ws}^{(0)}$ are updated based on $n_k^{\dagger}$, $x_k^{\dagger}, \forall k$ and $C_{\rm ws}^{\dagger}$, respectively, until the stopping condition is satisfied. After obtaining $\{n_k^{\triangle}\}$, we check if $\{n_k^{\triangle}\}$ is an integer set. If so, we set n_k^* as $n_k^{\triangle}$ for all k. If not, we obtain n_k^* by rounding each $n_k^{\triangle}$ to the nearest integer. Further, if $\{n_k^*\}$ cannot satisfy all constrains of $\mathbf{P_{1b}}$, we achieve $\{n_k^*\}$ by applying the proposed integer conversion method.

Algorithm 2 BCD based iterative algorithm for solving $\mathbf{P_1}$

Set the maximum error tolerance as ϵ_0 and the initial value of $\{\varepsilon_k\}$ as $\{\varepsilon_k^{(0)}\}$;
Initialize θ and set $\mathrm{Flag}=0$ and $\mathrm{Flag1}=0$;
repeat
  Solve $\mathbf{P_{1b}}$ by applying Algorithm 1 when letting $\varepsilon_k=\varepsilon_k^{(0)},\forall k$ and obtain the solution as $\{n_k^*\}$ and $\{\beta_k^{\triangle}\}$;
  Compute the corresponding sum throughput as $C_{\mathrm{ws}}^{\triangle}$;
  Compute the values of ε_k^+ for all k based on (15);
  if $C_{\mathrm{b},k}\big|_{\varepsilon_k=\varepsilon_k^+}\geq C_{\min,k}$ holds for all k **then**
    Compute $\varepsilon_k^{\diamond}$ by solving $C_{\mathrm{b},k}=C_{\min,k}$ within $\varepsilon_k\in\left[0,\varepsilon_k^+\right]$ for each k;
    if $C_{\mathrm{p}}|_{\varepsilon_k=\varepsilon_k^{\diamond},\forall k}-BTR_{\mathrm{p},0}=\Delta$ is met **then**
      Set $\varepsilon_k^*=\varepsilon_k^{\diamond},\forall k$ and $\mathrm{Flag}=1$;
    end if
    if $C_{\mathrm{p}}|_{\varepsilon_k=\varepsilon_k^+,\forall k}-BTR_{\mathrm{p},0}\geq\Delta$ **then**
      Set $\varepsilon_k^*=\varepsilon_k^+,\forall k$ and $\mathrm{Flag}=1$;
    end if
    if $\left(C_{\mathrm{p}}|_{\varepsilon_k=\varepsilon_k^{\diamond},\forall k}-BTR_{\mathrm{p},0}-\Delta\right)\left(C_{\mathrm{p}}|_{\varepsilon_k=\varepsilon_k^+,\forall k}-BTR_{\mathrm{p},0}-\Delta\right)<0$ **then**
      Set $\mathrm{Flag}=1$;
      repeat
        Compute $\varepsilon_k^*,\forall k$ with given θ based on (16) and update θ using the gradient method [30];
      until θ converges
    end if
  end if
  if $\mathrm{Flag}=1$ **then**
    Compute the corresponding sum throughput as C_{ws}^*;
    if $\left|C_{\mathrm{ws}}^{\triangle}-C_{\mathrm{ws}}^*\right|<\epsilon_0$ **then**
      Set $n_k^{\mathrm{o}}=n_k^*$, $\beta_k^{\mathrm{o}}=\beta_k^{\triangle}$ and $\varepsilon_k^{\mathrm{o}}=\varepsilon_k^*,\forall k$;
      Set $\mathrm{Flag1}=1$;
    else
      Set $\varepsilon_k^{(0)}=\varepsilon_k^*,\forall k$;
    end if
  else
    $\mathbf{P_1}$ is infeasible and set $\mathrm{Flag1}=1$;
  end if
until $\mathrm{Flag1}=1$

2) Algorithm 2 for solving $\mathbf{P_1}$*:* As shown in Algorithm 2, in each iteration, $\mathbf{P_{1b}}$ and $\mathbf{P_{1a}}$ are solved, obtaining the corresponding solutions[3]. Specifically, denote the initial value of ε_k as $\varepsilon_k^{(0)},\forall k$. Then we employ Algorithm 1 to solve $\mathbf{P_{1b}}$ by letting $\varepsilon_k=\varepsilon_k^{(0)},\forall k$, yielding the solution $\{n_k^*\}$ and $\{\beta_k^{\triangle}\}$. Accordingly, the weighted sum throughput under $\{n_k^*\}$ and $\{\beta_k^{\triangle}\}$ is determined by $C_{\mathrm{ws}}^{\triangle}$. Then by letting $n_k=n_k^*$ and $\beta_k=\beta_k^{\triangle},\forall k$, we first calculate the values of ε_k^+ for all k based on (15). Based on $\varepsilon_k^+,\forall k$, we further verify whether $\varepsilon_k^{\diamond}$ for each k exists within $\varepsilon_k\in\left[0,\varepsilon_k^+\right]$. If they all exist, compute $\varepsilon_k^{\diamond}$ for each k by solving $C_{\mathrm{b},k}=C_{\min,k}$ within $\varepsilon_k\in\left[0,\varepsilon_k^+\right]$. If not, $\mathbf{P_{1a}}$ is infeasible. If $\mathbf{P_{1a}}$ is feasible, any of the following three cases is satisfied, which are the case with $C_{\mathrm{p}}|_{\varepsilon_k=\varepsilon_k^{\diamond},\forall k}-BTR_{\mathrm{p},0}=\Delta$, the case with $C_{\mathrm{p}}|_{\varepsilon_k=\varepsilon_k^+,\forall k}-BTR_{\mathrm{p},0}\geq\Delta$ and the case with $\left(C_{\mathrm{p}}|_{\varepsilon_k=\varepsilon_k^{\diamond},\forall k}-BTR_{\mathrm{p},0}-\Delta\right)\left(C_{\mathrm{p}}|_{\varepsilon_k=\varepsilon_k^+,\forall k}-BTR_{\mathrm{p},0}-\Delta\right)<0$, respectively. Accordingly, we can compute the optimal solution $\{\varepsilon_k^*\}$ and the corresponding weighted sum throughput C_{ws}^*. When the stopping criterion $\left|C_{\mathrm{ws}}^{\triangle}-C_{\mathrm{ws}}^*\right|<\epsilon_0$ is met, we set the solution to $\mathbf{P_1}$ as $n_k^{\mathrm{o}}=n_k^*$, $\beta_k^{\mathrm{o}}=\beta_k^{\triangle}$ and $\varepsilon_k^{\mathrm{o}}=\varepsilon_k^*,\forall k$. Otherwise, we update $\varepsilon_k^{(0)}$ as ε_k^* for all k and repeat the above steps until the stopping criterion is satisfied.

[3]Note that $\mathbf{P_1}$ is infeasible if either $\mathbf{P_{1a}}$ or $\mathbf{P_{1b}}$ is infeasible in each iteration.

3) The convergence analysis for Algorithm 1 and Algorithm 2: Algorithm 1 is proposed based on the SCA method and the convergence of the SCA method has been proven in [34]. Based on the convergence of the SCA method, we provide a brief analysis for the convergence of Algorithm 1 as follows.

As pointed out in [35], the basic idea of the S-CA method is to obtain a locally optimal solution to the original non-convex problem by replacing its non-convex objective and constraints with their upper or lower bounds. Based on (17) and (20), $R_k^{\mathrm{up}}\left(x_k^{(0)},n_k^{(0)},x_k,n_k\right)$ and $C_k^{\mathrm{up}}\left(x_k^{(0)},n_k^{(0)},x_k,n_k\right)$ in $\mathbf{P_{3b}}$ are upper bounds for $R_k^{(2)}\left(x_k,n_k\right)$ and $\mathbb{E}_{x_{\mathrm{b},k}}\left[n_k\varepsilon_k\log_2\left(1+\frac{x_kb_k}{n_k}\right)\right]$. Therefore, the objective function of $\mathbf{P_{3b}}$ is a lower bound for that of $\mathbf{P_{2b}}$, while the feasible region in $\mathbf{P_{3b}}$ becomes a subset of that in $\mathbf{P_{2b}}$. That is, once the constraints $\mathrm{C1}-2$, $\mathrm{C2}-2$, $\mathrm{C3}-2$, $\mathrm{C4}-1$, $\mathrm{C5}-1$ and $\mathrm{C7}-1$ in $\mathbf{P_{3b}}$ are satisfied, the constraints $\mathrm{C1}-1$, $\mathrm{C2}-2$, $\mathrm{C3}-1$, $\mathrm{C4}-1$, $\mathrm{C5}-1$ and $\mathrm{C7}-1$ in $\mathbf{P_{2b}}$ must be satisfied. Therefore, $\mathbf{P_{2b}}$ is lower bounded by $\mathbf{P_{3b}}$. According to the convergence of the SCA method, the convergence of Algorithm 1 can also be guaranteed.

Algorithm 2 is proposed by means of the BCD method and its convergence can be proven as follows. Let $\left\{\{n_k^{*,j}\}_{k=1}^K,\{\beta_k^{\triangle,j}\}_{k=1}^K,\{\varepsilon_k^{*,j}\}_{k=1}^K\right\}$ denote the solution obtained in the j-th iteration. Denote $C_{\mathrm{ws,lb}}$ as the lower bound for C_{ws} due to the use of the first-order Taylor expansion. Then we have the following inequality

$$
\begin{aligned}
&C_{\mathrm{ws}}\left(\{n_k^{*,j}\}_{k=1}^K,\{\beta_k^{\triangle,j}\}_{k=1}^K,\{\varepsilon_k^{*,j}\}_{k=1}^K\right)\\
&\overset{(a)}{=}C_{\mathrm{ws,lb}}\left(\{n_k^{*,j}\}_{k=1}^K,\{\beta_k^{\triangle,j}\}_{k=1}^K,\{\varepsilon_k^{*,j}\}_{k=1}^K\right)\\
&\overset{(b)}{\leq}C_{\mathrm{ws,lb}}\left(\{n_k^{*,j+1}\}_{k=1}^K,\{\beta_k^{\triangle,j+1}\}_{k=1}^K,\{\varepsilon_k^{*,j}\}_{k=1}^K\right)\\
&\overset{(c)}{\leq}C_{\mathrm{ws}}\left(\{n_k^{*,j+1}\}_{k=1}^K,\{\beta_k^{\triangle,j+1}\}_{k=1}^K,\{\varepsilon_k^{*,j}\}_{k=1}^K\right)\\
&\overset{(d)}{\leq}C_{\mathrm{ws}}\left(\{n_k^{*,j+1}\}_{k=1}^K,\{\beta_k^{\triangle,j+1}\}_{k=1}^K,\{\varepsilon_k^{*,j+1}\}_{k=1}^K\right),
\end{aligned}
\tag{23}
$$

where (a) comes from the fact that the Taylor expansion in $R_k^{(2)}\left(x_k,n_k\right)\leq R_k^{\mathrm{up}}\left(x_k^{(0)},n_k^{(0)},x_k,n_k\right)$ is tight at the given local solution $\left\{\{n_k^{*,j}\}_{k=1}^K,\{\beta_k^{\triangle,j}\}_{k=1}^K\right\}$; (b) holds since $\left\{\{n_k^{*,j+1}\}_{k=1}^K,\{\beta_k^{\triangle,j+1}\}_{k=1}^K\right\}$ is the solution to $\mathbf{P_{1b}}$ by letting $\varepsilon_k=\varepsilon_k^{*,j},\forall k$; (c) always holds due to the fact that

$C_{\mathrm{ws,lb}}\left(\{n_k^{*,j+1}\}_{k=1}^K, \{\beta_k^{,j+1}\}_{k=1}^K, \{\varepsilon_k^{*,j}\}_{k=1}^K\right)$ is a lower bound for $C_{\mathrm{ws}}\left(\{n_k^{*,j+1}\}_{k=1}^K, \{\beta_k^{,j+1}\}_{k=1}^K, \{\varepsilon_k^{*,j}\}_{k=1}^K\right)$; and (d) holds as $\left\{\{\varepsilon_k^{*,j+1}\}_{k=1}^K\right\}$ is obtained by optimally solving $\mathbf{P_{1a}}$ while letting $n_k = n_k^{*,j+1}$ and $\beta_k = \beta_k^{\triangle,j+1}, \forall k$. The above inequality indicates that the weighted sum throughput of all IoT nodes is always non-decreasing after each iteration. Besides, it can be easily checked that the objective function of $\mathbf{P_1}$ has an upper bound due to the bounded optimization variables. As a result, Algorithm 2 is guaranteed to converge [35].

4) The computational complexity analysis of the proposed algorithm: The computational complexity of the proposed Algorithm 2 is analyzed as follows. Let $CC_{\mathbf{1a}}$ and $CC_{\mathbf{1b}}$ denote the computational complexities for solving $\mathbf{P_{1a}}$ and $\mathbf{P_{1b}}$, respectively. According to Algorithm 2, its computational complexity is given by

$$CC_{\mathbf{1}} = I_2\left(CC_{\mathbf{1a}} + CC_{\mathbf{1b}}\right), \tag{24}$$

where I_2 denotes the number of iterations for Algorithm 2 to converge.

As for $CC_{\mathbf{1a}}$, assume that the precision in the bisection search method is fixed as ϵ. Then the computational complexities for searching ε_k^{+} and $\varepsilon_k^{\diamond}, \forall k$ can be computed as $O\left(\log\left(\frac{\varepsilon_{\max}}{\epsilon}\right)\right)$ and $O\left(\log\left(\frac{\varepsilon_k^{+}}{\epsilon}\right)\right)$, respectively, where $O(\cdot)$ is the big-O notation [30]. Since $\mathbf{P_{2a}}$ is convex, the corresponding computational complexity can be computed as $O\left(\sqrt{2K+1}\log(2K+1)\right)$, where $2K+1$ denotes the number of inequality constraints in $\mathbf{P_{2a}}$ [30]. Therefore, $CC_{\mathbf{1a}}$ can be summarized as

$$CC_{\mathbf{1a}} = \begin{cases} KO\left(\log\left(\frac{\varepsilon_{\max}}{\epsilon}\right)\right), \text{case 1} \\ KO\left(\log\left(\frac{\varepsilon_{\max}}{\epsilon}\right)\right) + \sum_{k=1}^{K} O\left(\log\left(\frac{\varepsilon_k^{+}}{\epsilon}\right)\right), \text{case 2} \\ KO\left(\log\left(\frac{\varepsilon_{\max}}{\epsilon}\right)\right) + \sum_{k=1}^{K} O\left(\log\left(\frac{\varepsilon_k^{+}}{\epsilon}\right)\right) \\ +O\left(\sqrt{2K+1}\log(2K+1)\right), \text{case 3}, \end{cases} \tag{25}$$

where case 1 is the case with $C_{\mathrm{b},k}\big|_{\varepsilon_k=\varepsilon_k^{+}} \geq C_{\min,k}, \forall k$ and $C_{\mathrm{p}}\big|_{\varepsilon_k=\varepsilon_k^{+},\forall k} - BTR_{\mathrm{p},0} \geq \Delta$; case 2 is the case with $C_{\mathrm{b},k}\big|_{\varepsilon_k=\varepsilon_k^{+}} \geq C_{\min,k}, \forall k$ and $C_{\mathrm{p}}\big|_{\varepsilon_k=\varepsilon_k^{\diamond},\forall k} - BTR_{\mathrm{p},0} = \Delta$; and case 3 is the case with $C_{\mathrm{b},k}\big|_{\varepsilon_k=\varepsilon_k^{+}} \geq C_{\min,k}, \forall k$ and $\left(C_{\mathrm{p}}\big|_{\varepsilon_k=\varepsilon_k^{\diamond},\forall k} - BTR_{\mathrm{p},0} - \Delta\right)\left(C_{\mathrm{p}}\big|_{\varepsilon_k=\varepsilon_k^{+},\forall k} - BTR_{\mathrm{p},0} - \Delta\right) < 0$.

As for $CC_{\mathbf{1b}}$, the computational complexity for solving $\mathbf{P_{3b}}$ is given by $O\left(\sqrt{5K+2}\log(5K+2)\right)$ [30]. Then $CC_{\mathbf{1b}}$ is determined by

$$CC_{\mathbf{1b}} = I_1 O\left(\sqrt{5K+2}\log(5K+2)\right), \tag{26}$$

where I_1 denotes the number of iterations for Algorithm 1 to converge.

Substituting (25) and (26) into (24), the computational complexity of the proposed algorithm $CC_{\mathbf{1}}$ can be obtained.

Remark 3: It can be observed that $CC_{\mathbf{1}}$ increases with K, indicating that a larger number of IoT nodes will result in higher complexity in the proposed algorithm. However, the algorithm can still be a computationally efficient solution for large-scale IoT deployments. Specifically, in real-world IoT deployments, the PT within the MSR network can include base stations (BS), routers, user equipment (UE), and other devices [36]. Given the widespread deployment of these devices, it is feasible to establish numerous MSR networks across different regions, thereby enabling large-scale IoT implementations. Meanwhile, in each MSR network, the number of IoT nodes should be constrained for the following reasons. First, in a MSR network with K IoT nodes, the CR is required to execute the joint decoding scheme K times. Since the complexity of the joint decoding scheme is significantly higher than that of traditional decoding methods [24], limiting the number of IoT nodes in an MSR network is essential to reducing the CR's computational burden and the system's overall load. Second, increasing the number of IoT nodes in an MSR network could degrade the transmission performance of each node due to the limited availability of communication resources. Therefore, within each MSR network, the proposed algorithm can be employed to maximize the weighted sum throughput of all IoT nodes while maintaining low computational complexity.

Remark 4: This is the first work that investigates the weighted sum throughput maximization for the multi-IoT-node MSR network with hybrid long and short packets. In order to achieve this goal, we jointly optimize the EP, PRC and short-packet blocklength at multiple IoT nodes and then propose Algorithm 2 to obtain the corresponding resource allocation scheme. Besides, our proposed algorithm can also serve the following two purposes. Firstly, compared to the exhaustive search method, our proposed algorithm offers a method with lower complexity to achieve the near-optimal resource allocation that maximizes the weighted sum throughput of all IoT nodes in the investigated network[4]. Secondly, the proposed algorithm can be used to obtain the fixed EP scheme and the fixed PRC scheme. The former is designed to maximize the weighted sum throughput of all IoT nodes under a fixed EP at each IoT node, while the latter maximizes the weighted sum throughput assuming a fixed PRC at each IoT node. In particular, the fixed EP scheme is derived by solving $\mathbf{P_{1b}}$ via Algorithm 1. The fixed PRC scheme is implemented by employing Algorithm 2 to solve $\mathbf{P_1}$ with the fixed PRC.

IV. Simulation and Discussion

Here we evaluate the performance of the proposed resource allocation scheme in the considered network. Unless otherwise specified, the basic system parameters are set as shown in Table I following [5], [37]. Additionally, we adopt a standard channel fading model, where the channel gain for each link is represented as the product of the corresponding small-scale and large-scale fading components. Let d_0, $d_{1,k}$ and $d_{2,k}$ denote the distance of the primary link, and that from the

[4]For the exhaustive search method, let ϵ and ς denote the precision for searching ε_k and β_k for each k, respectively. Then the overall computational complexity of the exhaustive search method can be computed as $CC_{\mathrm{esm}} = O\left(\left(\frac{\varepsilon_{\max}}{\epsilon}\right)^K \left(\frac{1}{\varsigma}\right)^K A_{\lfloor N_{\mathrm{s}} \rfloor}^K\right)$, where $A_{\lfloor N_{\mathrm{s}} \rfloor}^K = \lfloor N_{\mathrm{s}} \rfloor \times (\lfloor N_{\mathrm{s}} \rfloor - 1) \times \cdots \times (\lfloor N_{\mathrm{s}} \rfloor - K + 1)$. By examining $CC_{\mathbf{1}}$ and CC_{esm}, it is evident that the computational complexity of the exhaustive search method is significantly higher than that of the proposed algorithm.

TABLE I
KEY SIMULATION SETTINGS

Parameters	Value
The given information transmission time budget T	1 s
The system bandwidth B	100 kHz
The number of the IoT nodes K	4
The constant circuit power at the k-th IoT node $P_{c,k}$	10 μW
The transmit power of the PT P_t	23 dBm
The number of the total channel uses N	10^5
The number of PT's signals within a short-packet signal M	128
The minimum effective throughput at the k-th IoT node $C_{\min,k}$	200 bits
The fixed energy conversion efficiency at each IoT node η	0.7
The minimum throughput gain for the primary transmission Δ	100 bits
The maximum tolerable EP at each IoT node $\varepsilon_{\max}$	0.1
The weight factors for all IoT nodes $\{w_k\}_{k=1}^{K}$	$\{0.2, 0.3, 0.3, 0.2\}$
The noise power density	-120 dBm/Hz

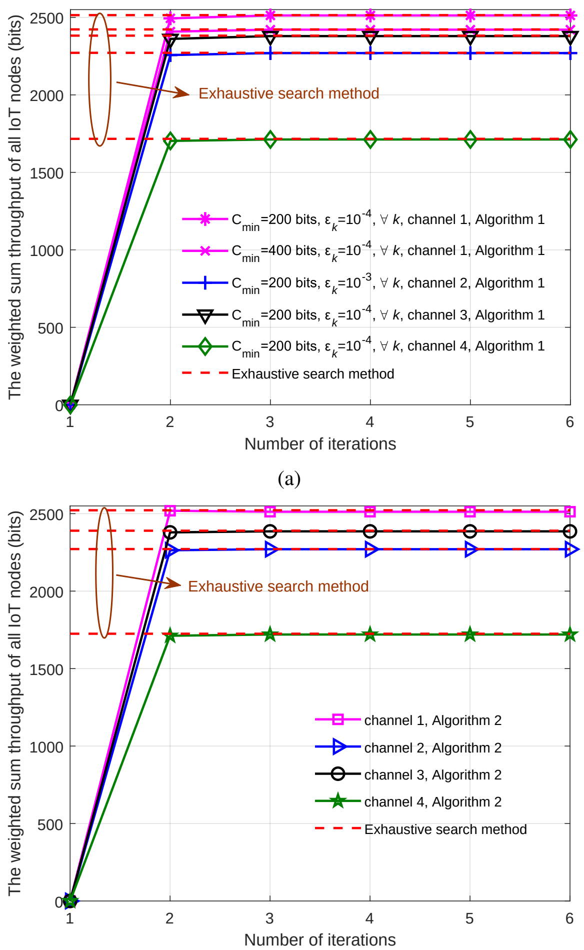

Fig. 2. The convergence and near-optimality of the proposed iterative algorithms: (a) the convergence and near-optimality of Algorithm 1; (b) the convergence and near-optimality of Algorithm 2.

k-th IoT node to the PT and the CR, respectively. Denote the path-loss exponent for each link as α. Then we set $d_0 = 55$ m, $d_{1,1} = d_{1,4} = 12$ m, $d_{1,2} = 15$ m, $d_{1,3} = 13$ m, $d_{2,1} = d_{2,4} = 45$ m, $d_{2,2} = 48$ m, $d_{2,3} = 46$ m and $\alpha = 3$.

A. Analysis for the Proposed Algorithms

Fig. 2 illustrates the convergence and near-optimality for both Algorithm 1 and Algorithm 2. Fig. 2(a) presents the convergence and near-optimality for Algorithm 1 under varying settings of the minimum effective throughput at each IoT node, denoted by $C_{\min}$, the EP of each IoT node and different channels. Specifically, we set $C_{\min}$ as 200 bits and 400 bits, respectively, and the EP of each IoT node as 10^{-4} and 10^{-3}. For the channels, we consider four randomly generated channel sets, denoted by channel 1, channel 2, channel 3 and channel 4. In order to illustrate the performance under Algorithm 1, we compare the weighted sum throughput of all IoT nodes achieved by Algorithm 1 with that under the exhaustive search method. It can be observed that the weighted sum throughput under Algorithm 1 is close to that under the exhaustive search method, illustrating the near-optimality of Algorithm 1. Another observation is that Algorithm 1 always achieves convergence in fewer than four iterations. This demonstrates that Algorithm 1 has a rapid convergence rate, indicating that Algorithm 1 is computationally efficient.

Fig. 2(b) shows the convergence and near-optimality of Algorithm 2 under varying channel settings. It can be observed that, regardless of the channel configuration, Algorithm 2 consistently converges to its maximum value after approximately three iterations, demonstrating its fast convergence rate. Additionally, the comparison between Algorithm 2 and the exhaustive search method shows the near-optimality of Algorithm 2.

B. Performance Analysis for the Proposed Scheme

In order to demonstrate the superiority of the proposed scheme, we evaluate its performance against the existing scheme optimized for LPC based multi-IoT-node MSR networks (referred to as LPC-MSR) in terms of the weighted sum throughput of all IoT nodes. In particular, the LPC-MSR scheme is optimized for LPC based multi-IoT-node MSR networks, where each IoT node performs LPC instead of SPC[5]. To ensure a fair comparison, we jointly optimize the PRC and backscatter time of each IoT node to maximize the weighted sum throughput, subject to the constraints on the QoS requirement and energy causality for each IoT node, as well as the PT's throughput gain. The optimal PRC and backscatter time at each IoT node are determined using the method outlined in [6]. Then we apply the obtained solution to the multi-IoT-node MSR network with hybrid long and short packets and verify whether the solution satisfies the constraints C1$-$C7. For convenience, we set $\varepsilon_k = 10^{-3}$ or 10^{-4} for all k. If these constraints are met, we recalculate the corresponding weighted sum throughput. Otherwise, the solution is deemed infeasible.

Besides, we include both the fixed EP and fixed PRC schemes in the performance comparison to assess the impacts of the EPs and PRCs at the IoT nodes on the weighted sum throughput. For the fixed EP scheme, the EP of each IoT node is set to 10^{-3} and 10^{-4}, respectively. For the fixed PRC scheme, the PRC of each IoT node is fixed as 0.5 and 0.9, respectively. As highlighted in Remark 3, both the fixed EP and fixed PRC schemes can be regarded as special cases of the proposed scheme, which are derived using the proposed algorithm.

[5]Due to the differences in the system model, optimization objectives, constraints, and BackCom power consumption between [23] and this work, it is not feasible to include the scheme in [23] in the performance comparison.

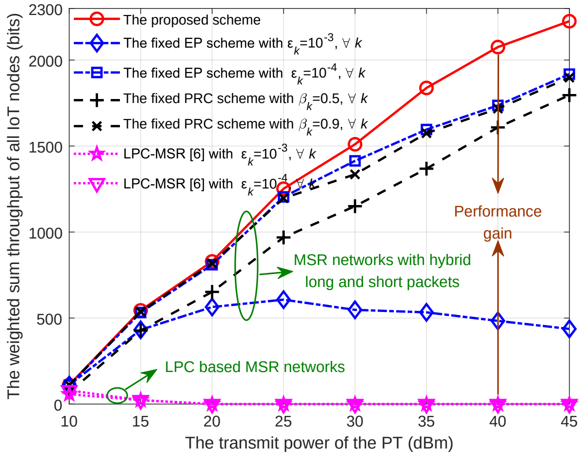

Fig. 3. The weighted sum throughput of all IoT nodes versus the transmit power of the PT P_{t}.

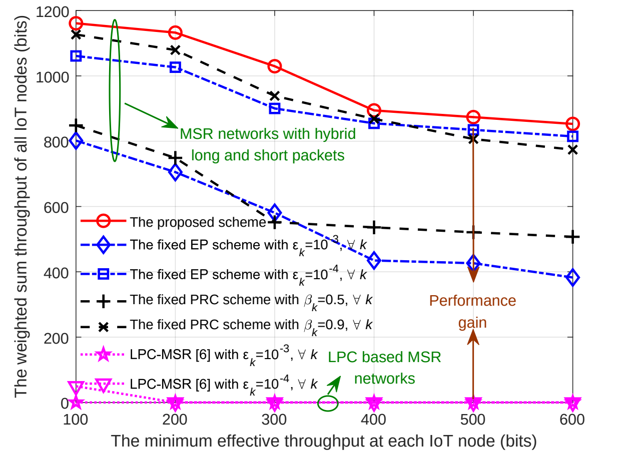

Fig. 4. The weighted sum throughput of all IoT nodes versus the minimum effective throughput at each IoT node $C_{\min}$.

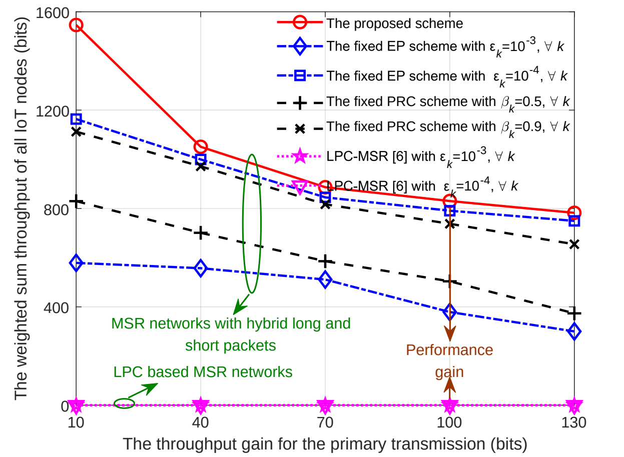

Fig. 5. The weighted sum throughput of all IoT nodes versus the minimum throughput gain for the primary transmission Δ.

Fig. 3 shows the weighted sum throughput of all IoT nodes C_{ws} versus the transmit power of the PT P_{t}, where the proposed scheme, the fixed EP scheme, the fixed PRC scheme and the LPC-MSR scheme are considered. Here P_{t} varies from 10 dBm to 45 dBm. It can be observed that as P_{t} increases, C_{ws} under the proposed scheme, the fixed EP scheme with $\varepsilon_k = 10^{-4}, \forall k$ and the fixed PRC scheme all increases. For the fixed EP scheme with $\varepsilon_k = 10^{-3}, \forall k$, C_{ws} initially rises before declining at higher P_{t} values. This occurs due to the following reasons. For the proposed scheme, the fixed EP scheme with $\varepsilon_k = 10^{-4}, \forall k$ or the fixed PRC scheme, the EP of each IoT node remains sufficiently small as P_{t} increases, ensuring that constraint C3 is satisfied. Under this condition, a higher P_{t} results in a stronger backscatter signal and higher harvested energy at each IoT node, bringing an enhancement to C_{ws}. For the fixed EP scheme with $\varepsilon_k = 10^{-3}, \forall k$, with a lower P_{t}, an increase in P_{t} strengthens the backscattered signal and increases the harvested energy, leading to an improvement in C_{ws}. However, when P_{t} reaches a sufficiently high level, constraint C3 may no longer be met, leading to a reduction in C_{ws}. In contrast, the LPC-MSR scheme exhibits a continuous decline in C_{ws} until it approaches zero. This is due to resource allocation mismatches that arise when the LPC-MSR scheme is applied to MSR networks with hybrid long and short packets, leading to unsatisfied constraints and a reduction in C_{ws}. By comparison, the proposed scheme consistently outperforms the LPC-MSR scheme in terms of C_{ws}, highlighting its superior performance. Furthermore, compared to the fixed EP and fixed PRC schemes, the proposed scheme always achieves a higher weighted sum throughput, especially when P_{t} becomes sufficiently large. This is attributed to the joint optimization of the EP, PRC and short-packet blocklength at each IoT node within the proposed scheme, which enables more flexible resource allocation, thereby optimizing C_{ws} more effectively.

Fig. 4 illustrates the weighted sum throughput of all IoT nodes C_{ws} as a function of the minimum effective throughput at each IoT node $C_{\min}$, where $C_{\min}$ ranges from 100 bits to 600 bits. It can be observed that as $C_{\min}$ increases, C_{ws} under the proposed scheme, the fixed EP scheme, the fixed PRC scheme and the LPC-MSR scheme initially decreases sharply, and then the rate of decline gradually slows down. This behavior can be attributed to the following reasons. When $C_{\min}$ is small, the QoS constraint can easily be met at each IoT node and a smaller $C_{\min}$ allows more resources to be allocated to IoT nodes with better channel conditions, which significantly improves C_{ws}. When $C_{\min}$ becomes sufficiently large, the IoT nodes with poorer channel conditions will be allocated more resources to meet their throughput requirements, which leads to better throughput fairness among the IoT nodes but also results in a slight reduction in C_{ws}. Compared to the other schemes, the proposed scheme always achieves the highest weighted sum throughput, demonstrating its superiority. Besides, the LPC-MSR scheme appears ill-suited for the considered network, resulting in the poorest performance.

Fig. 5 shows the effect of the minimum throughput gain for the primary transmission Δ on the weighted sum throughput of all IoT nodes C_{ws}, where $C_{\min}$ is set to 640 bits and Δ ranges from 10 bits to 130 bits. It is evident that as Δ increases, C_{ws} for the proposed scheme, the fixed EP scheme and the fixed PRC scheme decreases, while C_{ws} for the LPC-MSR scheme

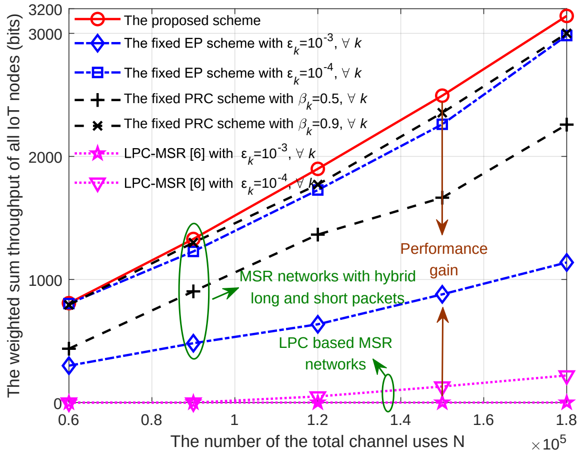

Fig. 6. The weighted sum throughput of all IoT nodes versus the number of the total channel uses N.

remains zero. This behavior can be explained as follows. A larger Δ makes it more challenging to satisfy constraint C3. In order to guarantee it, more resources must be allocated to IoT nodes that provide higher throughput gains for the primary transmission, leading to a reduction in $C_{\rm ws}$. In the case of the LPC-MSR scheme, not all constraints can be satisfied, leading to $C_{\rm ws} = 0$. In contrast, the proposed scheme achieves the highest weighted sum throughput while the LPC-MSR scheme exhibits the poorest performance, highlighting the superiority of the proposed scheme and exposing the resource allocation mismatches inherent in the LPC-MSR scheme when applied to the considered network.

In Fig. 6, the weighted sum throughput of all IoT nodes $C_{\rm ws}$ is plotted against the number of the total channel uses N, where N ranges from 6×10^4 to 1.8×10^5 and $P_{\rm t}$ is set as 30 dBm. It is observed that $C_{\rm ws}$ increases with N for all schemes. This can be attributed to the following reason. An increase in N indicates that more short-packet blocklengths can be allocated to the IoT nodes for improving their throughput, which enhances $C_{\rm ws}$. In contrast, the proposed scheme consistently yields the highest weighted sum throughput, thereby showing its advantage. It is worth noting that both the fixed EP and fixed PRC schemes perform close to the proposed scheme as they represent special cases of the proposed scheme and can be derived from the proposed algorithm. On the other hand, the LPC-MSR scheme is poorly adapted to the considered network, leading to the least favorable performance.

V. Conclusions

In this work, we have investigated the multi-IoT-node MSR network with hybrid long and short packets. Considering the EPs of the IoT nodes, we have derived the lower bound expression of the primary transmission rate. Then we have proposed a resource allocation scheme to maximize the weighted sum throughput of all IoT nodes while ensuring the throughput gain for the primary transmission. Simulation results confirmed that the proposed iterative algorithm exhibits a rapid convergence rate and demonstrated that our proposed scheme outperforms the existing scheme in terms of the weighted sum throughput of all IoT nodes. Additionally, we obtained the following findings. Firstly, the existence of the EP at each IoT node may destroy the mutual benefits between the primary transmission and the IoT nodes' BackCom, particularly when the EP of the IoT node is large. Based on this finding, by carefully selecting the appropriate EP for each IoT node, it becomes possible to restore the mutualistic relationship. Secondly, the weighted sum throughput is maximized when all IoT nodes either participate in sequential short-packet BackCom throughout the given information transmission time budget or exhaust (or almost exhaust) all their harvested energy for BackCom. Thirdly, the existing scheme designed for LPC based MSR results in resource allocation mismatches in MSR employing hybrid long and short packets, leading to a poor performance. Therefore, it is essential to develop and implement new resource allocation strategies specifically tailored for MSR networks with hybrid long and short packets.

Appendix A

By relaxing the integer variable n_k to the continue one, we can take the first-order derivative of $C_{\rm ws}$ with respect to n_k, which is given by

$$\frac{\partial C_{\rm ws}}{\partial n_k} = A_k\left(\log_2\left(1+\gamma_k\right) - \frac{n_k^{-\frac{1}{2}}}{2}\sqrt{V\left(\gamma_k\right)}Q^{-1}\left(\varepsilon_k\right)\right), \quad \text{(A.1)}$$

where $A_k = w_k\left(1-\varepsilon_k\right)$. It can be observed that whether $\frac{\partial C_{\rm ws}}{\partial n_k} \geq 0$ or not depends on the sign of $f_k(n_k)$, where $f_k(n_k) = \log_2\left(1+\gamma_k\right) - \frac{n_k^{-\frac{1}{2}}}{2}\sqrt{V\left(\gamma_k\right)}Q^{-1}\left(\varepsilon_k\right)$.

In order to ensure C1, we have

$$\log_2\left(1+\gamma_k\right) - \sqrt{\frac{V\left(\gamma_k\right)}{n_k}}Q^{-1}\left(\varepsilon_k\right) \geq \frac{C_{\min,k}}{\left(1-\varepsilon_k\right)n_k} > 0. \quad \text{(A.2)}$$

Since $f_k(n_k) = \log_2\left(1+\gamma_k\right) - \sqrt{\frac{V(\gamma_k)}{n_k}}Q^{-1}\left(\varepsilon_k\right) + \frac{n_k^{-\frac{1}{2}}}{2}\sqrt{V\left(\gamma_k\right)}Q^{-1}\left(\varepsilon_k\right) > \log_2\left(1+\gamma_k\right) - \sqrt{\frac{V(\gamma_k)}{n_k}}Q^{-1}\left(\varepsilon_k\right) > 0$, we can obtain $\frac{\partial C_{\rm ws}}{\partial n_k} > 0$. Thus, $C_{\rm ws}$ always increases as n_k increases, even when n_k is an integer.

Considering the monotonically increasing behavior of $C_{\rm ws}$ with respect to n_k, the maximum $C_{\rm ws}$ is achieved when $n_k^{\ddagger}$ is decided by its upper bound. By observing all constraints of $\mathbf{P_0}$, the upper bound of n_k depends on C2 and C4. Specifically, based on C2, we have $n_k \leq \frac{N_{\rm s}}{B_k+\beta_k}$ with $B_k = \frac{P_{{\rm c},k}}{\eta P_{\rm t} h_{1,k}}, \forall k$. When $\sum_{k=1}^{K}\left\lfloor \frac{N_{\rm s}}{B_k+\beta_k}\right\rfloor > \lfloor N_{\rm s}\rfloor$ is satisfied, we have $\sum_{k=1}^{K} n_k^{\ddagger} = \lfloor N_{\rm s}\rfloor$. Otherwise, $n_k^{\ddagger}$ is determined by $\lfloor \frac{N_{\rm s}}{B_k+\beta_k}\rfloor, \forall k$. Therefore, Lemma 1 can be proven.

Appendix B

Letting $C_k = n_k w_k \log_2\left(1+\gamma_k\right)$ and $D_k = w_k\sqrt{n_k V\left(\gamma_k\right)}, \forall k$, $C_{\rm ws}$ can be written as $\sum_{k=1}^{K}\left(1-\varepsilon_k\right)\left(C_k - D_k Q^{-1}\left(\varepsilon_k\right)\right)$. Then taking the first-order derivative of $C_{\rm ws}$ with respect to ε_k, we have

$$\frac{\partial C_{\rm ws}}{\partial \varepsilon_k} = D_k Q^{-1}\left(\varepsilon_k\right) - \left(1-\varepsilon_k\right) D_k \frac{\partial Q^{-1}\left(\varepsilon_k\right)}{\partial \varepsilon_k} - C_k, \quad \text{(B.1)}$$

where $\frac{\partial Q^{-1}(\varepsilon_k)}{\partial \varepsilon_k} = -\sqrt{2\pi}\exp\left(\frac{1}{2}\left(Q^{-1}\left(\varepsilon_k\right)\right)^2\right)$ denotes the first-order derivative of $Q^{-1}\left(\varepsilon_k\right)$ in terms of ε_k. Based on (B.1), we can calculate the second-order derivative of $C_{\rm ws}$ as

$$\frac{\partial^2 C_{\rm ws}}{\partial \varepsilon_k^2} = 2D_k \frac{\partial Q^{-1}\left(\varepsilon_k\right)}{\partial \varepsilon_k} - \left(1-\varepsilon_k\right) D_k \frac{\partial^2 Q^{-1}\left(\varepsilon_k\right)}{\partial \varepsilon_k^2}, \quad \text{(B.2)}$$

where $\frac{\partial^2 Q^{-1}(\varepsilon_k)}{\partial \varepsilon_k^2} = 2\pi Q^{-1}\left(\varepsilon_k\right)\exp\left(\left(Q^{-1}\left(\varepsilon_k\right)\right)^2\right)$ is the second-order derivative of $Q^{-1}\left(\varepsilon_k\right)$.

Since both $\frac{\partial Q^{-1}(\varepsilon_k)}{\partial \varepsilon_k} < 0$ and $\frac{\partial^2 Q^{-1}(\varepsilon_k)}{\partial \varepsilon_k^2} > 0$ always hold, we obtain $\frac{\partial^2 C_{\rm ws}}{\partial \varepsilon_k^2} < 0$. Thus, $C_{\rm ws}$ is a concave function with respect to $\varepsilon_k, \forall k$. Accordingly, C1 is a convex constraint. Considering that both C3 and C6 are linear constraints, $\mathbf{P_{1a}}$ is a convex optimization problem. Then the proof is finalized.

Appendix C

Let θ denote the non-negative Lagrange multiplier with respect to C3. Then the dual problem for $\mathbf{P_{2a}}$ under the case with $\left(C_{\rm p}|_{\varepsilon_k=\varepsilon_k^{\diamond},\forall k} - BTR_{{\rm p},0} - \Delta\right)\left(C_{\rm p}|_{\varepsilon_k=\varepsilon_k^{+},\forall k} - BTR_{{\rm p},0} - \Delta\right) < 0$ is given by

$$\begin{aligned} &\max_{\boldsymbol{\varepsilon},\theta} \ \ \mathcal{L}(\boldsymbol{\varepsilon},\theta) \\ &\text{s.t. C8}, \end{aligned} \quad \text{(C.1)}$$

where $\mathcal{L}(\boldsymbol{\varepsilon},\theta) = C_{\rm ws} + \theta\left(C_{\rm p} - BTR_{{\rm p},0} - \Delta\right)$.

Taking the first-order derivative of $\mathcal{L}(\boldsymbol{\varepsilon},\theta)$ in terms of ε_k, we have $\frac{\partial \mathcal{L}(\varepsilon,\theta)}{\partial \varepsilon_k} = F_k\left(\varepsilon_k\right) - \theta\omega_k$, where $\omega_k = BT_{\rm b} n_k \mathbb{E}_{x_{{\rm b},k}}\!\left[\log_2\!\left(1+\gamma_{\rm p}^{\rm s}\left(x_{{\rm b},k}\right)\right) - \log_2\!\left(1+\gamma_{\rm p}^{\rm f}\left(x_{{\rm b},k}\right)\right)\right]$. Since $\frac{\partial^2 \mathcal{L}(\varepsilon,\theta)}{\partial \varepsilon_k^2} = \frac{\partial F_k(\varepsilon_k)}{\partial \varepsilon_k} = \frac{\partial^2 C_{\rm ws}}{\partial \varepsilon_k^2} < 0$, $\frac{\partial \mathcal{L}(\varepsilon,\theta)}{\partial \varepsilon_k}$ is monotonically decreasing as ε_k increases. Accordingly, the optimal ε_k to (C.1) is given by (16). Therefore, Proposition 2 is obtained.

Appendix D

As shown in $\mathbf{P_{2b}}$, we observe that $\mathrm{C2}-2$, $\mathrm{C4}-1$, $\mathrm{C5}-1$ and $\mathrm{C7}-1$ are linear. Therefore, $\mathbf{P_{2b}}$ is convex if the objective function is concave and constraints $\mathrm{C1}-1$ and $\mathrm{C3}-1$ are convex.

For the objective function and constraint $\mathrm{C1}-1$, both $R_k^{(1)}\left(x_k,n_k\right)$ and $R_k^{(2)}\left(x_k,n_k\right)$ exist. Specifically, if $R_k^{(1)}\left(x_k,n_k\right)$ is a concave function and $R_k^{(2)}\left(x_k,n_k\right)$ is convex, then we can prove that the objective function is concave and $\mathrm{C1}-1$ is a convex constraint. Using the fact that the perspective function can preserve convexity, the convexity of $R_k^{(1)}\left(x_k,n_k\right)$ is the same as that of $\log_2\left(1+a_k x_k\right)$. Since $\log_2\left(1+a_k x_k\right)$ is a concave function, $R_k^{(1)}\left(x_k,n_k\right)$ can also be proven as concave.

Letting $y_k = \frac{a_k x_k}{n_k}$, we take the second-order derivatives of $R_k^{(2)}\left(x_k,n_k\right)$ with respect to x_k and n_k as

$$\frac{\partial^2 R_k^{(2)}\left(x_k,n_k\right)}{\partial x_k^2} = -\frac{E_{1,k} a_k \left(V(y_k)^{-1} + 3(1+y_k)^2\right)}{\left(1+y_k\right)^6}, \quad \text{(D.1)}$$

$$\frac{\partial^2 R_k^{(2)}\left(x_k,n_k\right)}{\partial n_k^2} = -\frac{E_{1,k}}{2a_k}\left(\frac{V\left(y_k\right)^{-1} E_{2,k}^2}{2} + \frac{6y_k^2}{\left(1+y_k\right)^4}\right), \quad \text{(D.2)}$$

where $E_{1,k} = n_k^{-\frac{3}{2}} Q^{-1}\left(\varepsilon_k\right) a_k V(y_k)^{-\frac{1}{2}}$ and $E_{2,k} = V\left(y_k\right) - \frac{2y_k}{(1+y_k)^3}$. Taking the partial derivative of $R_k^{(2)}\left(x_k,n_k\right)$ in terms of x_k and n_k, we have

$$\frac{\partial^2 R_k^{(2)}\left(x_k,n_k\right)}{\partial x_k \partial n_k} = E_{1,k}\left(\frac{-V\left(y_k\right)^{-1} E_{2,k}}{2\left(1+y_k\right)^3} + \frac{3y_k}{\left(1+y_k\right)^4}\right). \quad \text{(D.3)}$$

Likewise, we have $\frac{\partial^2 R_k^{(2)}(x_k,n_k)}{\partial n_k \partial x_k} = \frac{\partial^2 R_k^{(2)}(x_k,n_k)}{\partial x_k \partial n_k}$.

Then the Hessian matrix of $R_k^{(2)}\left(x_k,n_k\right)$ is given by

$$\nabla^2 R_k^{(2)}\left(x_k,n_k\right) = \begin{bmatrix} \frac{\partial^2 R_k^{(2)}(x_k,n_k)}{\partial x_k^2} & \frac{\partial^2 R_k^{(2)}(x_k,n_k)}{\partial x_k \partial n_k} \\ \frac{\partial^2 R_k^{(2)}(x_k,n_k)}{\partial n_k \partial x_k} & \frac{\partial^2 R_k^{(2)}(x_k,n_k)}{\partial n_k^2} \end{bmatrix}. \quad \text{(D.4)}$$

Since $\frac{\partial^2 R_k^{(2)}(x_k,n_k)}{\partial x_k^2} < 0$ due to $E_{1,k} > 0$, the second-order principal minor of $\nabla^2 R_k^{(2)}\left(x_k,n_k\right)$ is given by

$$\begin{aligned} &\frac{\partial^2 R_k^{(2)}\left(x_k,n_k\right)}{\partial x_k^2} \times \frac{\partial^2 R_k^{(2)}\left(x_k,n_k\right)}{\partial n_k^2} - \left(\frac{\partial^2 R_k^{(2)}\left(x_k,n_k\right)}{\partial x_k \partial n_k}\right)^2 = E_{1,k}^2 \\ &\times 3V(y_k)^{-1}\left(\frac{E_{2,k}^2}{4(1+y_k)^4} + \frac{y_k^2}{\left(1+y_k\right)^{10}} + \frac{y_k E_{2,k}}{\left(1+y_k\right)^7}\right) > 0. \quad \text{(D.5)} \end{aligned}$$

Thus, $R_k^{(2)}\left(x_k,n_k\right)$ is a concave function.

For constraint $\mathrm{C3}-1$, $C'_{{\rm p},k}$ includes two concave functions, which are $n_k \mathbb{E}_{x_{{\rm b},k}}\left[\log_2\left(1+\frac{P_{\rm t} h_0}{\sigma^2} + \frac{x_k b_k}{n_k}\right)\right]$ and $\mathbb{E}_{x_{{\rm b},k}}\left[n_k \varepsilon_k \log_2\left(1+\frac{x_k b_k}{n_k}\right)\right]$, respectively.

Therefore, the difference of two concave functions exists in both the objective function and constraints $\mathrm{C1}-1$ and $\mathrm{C3}-1$, resulting in the non-convexity of $\mathbf{P_{2b}}$. Accordingly, the proof of Proposition 3 is complete.

References

[1] L. Chettri and R. Bera, “A comprehensive survey on internet of things (IoT) toward 5G wireless systems,” *IEEE Internet Things J.*, vol. 7, no. 1, pp. 16–32, 2020.

[2] R. Xu, Y. Ye, H. Sun, L. Shi, and G. Lu, “Revolutionizing symbiotic radio: Exploiting tradeoffs in hybrid active-passive communications,” *arXiv preprint arXiv:2504.18168*, 2025.

[3] Y. Ye, L. Shi, X. Chu, and G. Lu, “On the outage performance of ambient backscatter communications,” *IEEE Internet Things J.*, vol. 7, no. 8, pp. 7265–7278, 2020.

[4] Q. Zhang, Y.-C. Liang, H.-C. Yang, and H. V. Poor, “Mutualistic mechanism in symbiotic radios: When can the primary and secondary transmissions be mutually beneficial?” *IEEE Trans. Wireless Commun.*, vol. 21, no. 10, pp. 8036–8050, 2022.

[5] R. Long, Y.-C. Liang, H. Guo, G. Yang, and R. Zhang, “Symbiotic radio: A new communication paradigm for passive internet of things,” *IEEE Internet Things J.*, vol. 7, no. 2, pp. 1350–1363, 2020.

[6] Y. Ye, L. Shi, X. Chu, G. Lu, and S. Sun, “Mutualistic cooperative ambient backscatter communications under hardware impairments,” *IEEE Trans. Commun.*, vol. 70, no. 11, pp. 7656–7668, 2022.

[7] H. Yang, Y. Ye, K. Liang, and X. Chu, “Energy efficiency maximization for symbiotic radio networks with multiple backscatter devices,” *IEEE Open J. Commun. Soc.*, vol. 2, pp. 1431–1444, 2021.

[8] Q. Zhang, Y.-C. Liang, and H. V. Poor, “Reconfigurable intelligent surface assisted MIMO symbiotic radio networks,” *IEEE Trans. Commun.*, vol. 69, no. 7, pp. 4832–4846, 2021.

[9] Z. Tu, R. Long, Y. Pei, and Y.-C. Liang, “RIS-enabled full-duplex backscatter communication in multi-user symbiotic radio,” *IEEE Trans. Wireless Commun.*, pp. 1–1, 2024.

[10] S. Wang, J. Xu, and Y. Zeng, “On the energy-efficiency trade-off between active and passive communications with RIS-based symbiotic radio,” *IEEE Trans. Green Commun. Netw.*, pp. 1–1, 2024.

[11] C. Zhou, Y. Xu, D. Li, C. Huang, C. Yuen, J. Zhou, and G. Yang, "Energy-efficient maximization for RIS-aided MISO symbiotic radio systems," *IEEE Trans. Veh. Technol.*, vol. 72, no. 10, pp. 13 689–13 694, 2023.

[12] P. Du, Z. Chang, and Y.-C. Liang, "Joint active and passive beamforming for physical layer security in mmwave symbiotic radio system," *IEEE Wireless Commun. Lett.*, pp. 1–1, 2024.

[13] B. Lyu, C. Zhou, S. Gong, D. T. Hoang, and Y.-C. Liang, "Robust secure transmission for active RIS enabled symbiotic radio multicast communications," *IEEE Trans. Wireless Commun.*, vol. 22, no. 12, pp. 8766–8780, 2023.

[14] J. Hu, Y.-C. Liang, Y. Pei, S. Sun, and R. Liu, "Reconfigurable intelligent surface based uplink MU-MIMO symbiotic radio system," *IEEE Trans. Wireless Commun.*, vol. 22, no. 1, pp. 423–438, 2023.

[15] Y. Zhang, L. Lv, L. Yang, Y. Xu, Z. Ding, and J. Chen, "Symbiotic NOMA: A mutualism communication paradigm toward green massive access," *IEEE Commun. Lett.*, vol. 28, no. 10, pp. 2437–2441, 2024.

[16] X. Lu, P. Wang, G. Li, D. Niyato, and Z. Li, "Short-packet backscatter assisted wireless-powered relaying with NOMA: Mode selection with performance estimation," *IEEE Trans. Cogn. Commun. Netw.*, vol. 8, no. 1, pp. 216–231, 2022.

[17] Y. Polyanskiy, H. V. Poor, and S. Verdu, "Channel coding rate in the finite blocklength regime," *IEEE Trans. Inf. Theory*, vol. 56, no. 5, pp. 2307–2359, 2010.

[18] G. Durisi, T. Koch, and P. Popovski, "Toward massive, ultrareliable, and low-latency wireless communication with short packets," *Proc. IEEE*, vol. 104, no. 9, pp. 1711–1726, 2016.

[19] J. Shi, L. Shi, Y. Ye, Y. Zhang, and X. Chu, "Performance analysis for ambient backscatter communications with hybrid long-short packets," *IEEE Wireless Commun. Lett.*, vol. 13, no. 5, pp. 1325–1329, 2024.

[20] Z. Zhao, Y. Cai, W. Hong, J. Jiang, M. Peng, and T. Q. S. Quek, "On the design of backscatter communications with retransmissions," *IEEE Wireless Commun. Lett.*, vol. 11, no. 12, pp. 2555–2559, 2022.

[21] L. Shi, J. Shi, Y. Ye, G. Zheng, and G. Lu, "Ambient backscatter communication with HARQ assisted hybrid long-short packets," *IEEE Commun. Lett.*, vol. 28, no. 10, pp. 2258–2262, 2024.

[22] X. Song, D. Han, L. Shi, H. Sun, and R. Q. Hu, "Relay assisted cooperative ambient backscatter communication with hybrid long-short packets," *IEEE Trans. Veh. Technol.*, vol. 73, no. 9, pp. 12 890–12 903, 2024.

[23] Z. Chu, W. Hao, P. Xiao, M. Khalily, and R. Tafazolli, "Resource allocations for symbiotic radio with finite blocklength backscatter link," *IEEE Internet Things J.*, vol. 7, no. 9, pp. 8192–8207, 2020.

[24] Y.-C. Liang, Q. Zhang, E. G. Larsson, and G. Y. Li, "Symbiotic radio: Cognitive backscattering communications for future wireless networks," *IEEE Trans. Cogn. Commun. Netw.*, vol. 6, no. 4, pp. 1242–1255, 2020.

[25] D. Xu, H. Zhao, and H. Zhu, "Resource allocation for secure short packet communications in wireless powered IoT networks," *IEEE Trans. Veh. Technol.*, vol. 72, no. 8, pp. 11 000–11 005, 2023.

[26] J. Chen, L. Zhang, Y.-C. Liang, X. Kang, and R. Zhang, "Resource allocation for wireless-powered IoT networks with short packet communication," *IEEE Trans. Wireless Commun.*, vol. 18, no. 2, pp. 1447–1461, 2019.

[27] M. Oh, J. Park, and J. Choi, "Joint optimization for secure and reliable communications in finite blocklength regime," *IEEE Trans. Wireless Commun.*, vol. 22, no. 12, pp. 9457–9472, 2023.

[28] Z. B. Zawawi, Y. Huang, and B. Clerckx, "Multiuser wirelessly powered backscatter communications: Nonlinearity, waveform design, and SINR-energy tradeoff," *IEEE Trans. Wireless Commun.*, vol. 18, no. 1, pp. 241–253, 2019.

[29] Y. Ye, Y. Li, Z. Wang, X. Chu, and H. Zhang, "Dynamic asymmetric power splitting scheme for SWIPT-based two-way multiplicative AF relaying," *IEEE Signal Process. Lett.*, vol. 25, no. 7, pp. 1014–1018, 2018.

[30] S. Boyd and L. Vandenberghe, *Convex Optimization*. Cambridge, U.K.:Cambridge Univ. Press, 2004.

[31] Z. Yin, N. Cheng, T. H. Luan, Y. Song, and W. Wang, "DT-assisted multi-point symbiotic security in space-air-ground integrated networks," *IEEE Trans. Inf. Forensics Security*, vol. 18, pp. 5721–5734, 2023.

[32] Z. Yin, N. Cheng, T. H. Luan, Y. Hui, and W. Wang, "Green interference based symbiotic security in integrated satellite-terrestrial communications," *IEEE Trans. Wireless Commun.*, vol. 21, no. 11, pp. 9962–9973, 2022.

[33] Z. Yin, N. Cheng, Y. Hui, W. Wang, L. Zhao, K. Aldubaikhy, and A. Alqasir, "Multi-domain resource multiplexing based secure transmission for satellite-assisted IoT: AO-SCA approach," *IEEE Trans. Wireless Commun.*, vol. 22, no. 11, pp. 7319–7330, 2023.

[34] A. B.-T. A. Beck and L. Tetruashvili, "A sequential parametric convex approximation method with applications to nonconvex truss topology design problems," *J. Glob. Optim.*, vol. 47, no. 1, pp. 29–51, 2010.

[35] G. Yang, R. Dai, and Y.-C. Liang, "Energy-efficient UAV backscatter communication with joint trajectory design and resource optimization," *IEEE Trans. Wireless Commun.*, vol. 20, no. 2, pp. 926–941, 2021.

[36] M. M. Butt, N. R. Mangalvedhe, N. K. Pratas, J. Harrebek, J. Kimionis, M. Tayyab, O.-E. Barbu, R. Ratasuk, and B. Vejlgaard, "Ambient IoT: A missing link in 3GPP IoT devices landscape," *IEEE Internet Things Mag.*, vol. 7, no. 2, pp. 85–92, 2024.

[37] L. Shi, X. Chu, H. Sun, and G. Lu, "Wireless-powered OFDMA-MEC networks with hybrid activepassive communications," *IEEE Internet Things J.*, vol. 10, no. 12, pp. 10 484–10 496, 2023.